IEEE Access
Multidisciplinary ⋮ Rapid Review ⋮ Open Access Journal

Received 9 October 2023, accepted 7 November 2023, date of publication 9 November 2023, date of current version 20 November 2023.

Digital Object Identifier 10.1109/ACCESS.2023.3331760

RESEARCH ARTICLE

Single-Objective Optimal Design of a High-Performance Wind Turbine Airfoil Family

ZHAOHUANG ZHANG, DI GAO, YUNFEI QI, AND KEFENG CHENG
Department of Energy Power and Mechanical Engineering, North China Electric Power University, Beijing 102206, China
Corresponding author: Di Gao (120192102117@ncepu.edu.cn)

ABSTRACT The development of high-performance wind turbine blade airfoil families is an important research topic in wind power generation technology. Using the NACA63 series airfoil as the initial airfoil, the XFOIL software based on the panel method is used to calculate the airfoil's lift-drag coefficient. Secondly, an improved Hicks-Henne shape function is employed to define the airfoil's geometry. Finally, a single objective optimization model is established based on three optimization algorithms (genetic algorithm, particle swarm optimization algorithm, and particle swarm optimization and genetic algorithm), which takes the control coefficient of shape function as a variable, the maximum of lift coefficient and lift-drag ratio as the goal, and satisfies the geometric and aerodynamic constraints. Different angles of attack, Reynolds numbers and weight coefficients are considered, there are seven groups high-performance airfoil families obtained (ZDGN-ASG, ZDGN-ASP, ZDGN-ASPG, ZDGN-ASR1, ZDGN-ASR5, ZDGN-ASQ3, ZDGN-ASQ8). The lift coefficients and lift-to-drag ratios are higher than those of the initial airfoil under the same operating conditions, and have been applied to the actual 1.2MW wind turbine blades. The results show that the output power and wind energy utilization coefficient of the new blades are significantly improved, further proving that the new airfoil family has superior aerodynamic performance.

INDEX TERMS Wind turbine, airfoil family, high performance, single objective, optimal design, aerodynamic performance.

I. INTRODUCTION

Energy is an important material basis for the survival and development of human society, is crucial to economic development, social progress and national security, and occupies a major position in the development strategies of all countries [1]. With the rapid development of the economy, fossil energy sources are becoming increasingly depleted and environmental problems are becoming more and more prominent. Wind energy, which is a renewable new energy source, is gradually gaining popularity because of its abundant reserves and non-polluting characteristics, while the development of wind power generation technology is an important way to alleviate energy shortage and reduce environmental pollution [2]. Wind turbines are the key power equipment in wind power generation technology, and the blade, as the core component of the wind turbine to capture wind energy, the aerodynamic performance of its airfoil is a fundamental factor in determining the power characteristics and load characteristics of the wind turbine [3]. Therefore, the design and development of a special airfoil family to meet the performance requirements of wind turbines are of great significance to improve the efficiency of wind turbines and use wind energy resources safely as well as reliably.

In the early days, wind turbine airfoils were mainly selected from aviation low-speed airfoils, such as the US NACA series [4], but with the development of wind power generation technology, it was gradually found that due to different operating conditions, aviation airfoils were not well suited to meet the requirements of the special operating environment of wind turbines, so various countries developed their own special airfoil families for wind turbines, such as the US NREL-S series [5], the Swedish FFA-W series [6], the Dutch DU series [7], the Danish RISΦ series [8] and the Chinese NPU-WA series [9], etc., as shown in Fig. 1. These airfoils have been widely used on various types of

The associate editor coordinating the review of this manuscript and approving it for publication was Ehab Elsayed Elattar.

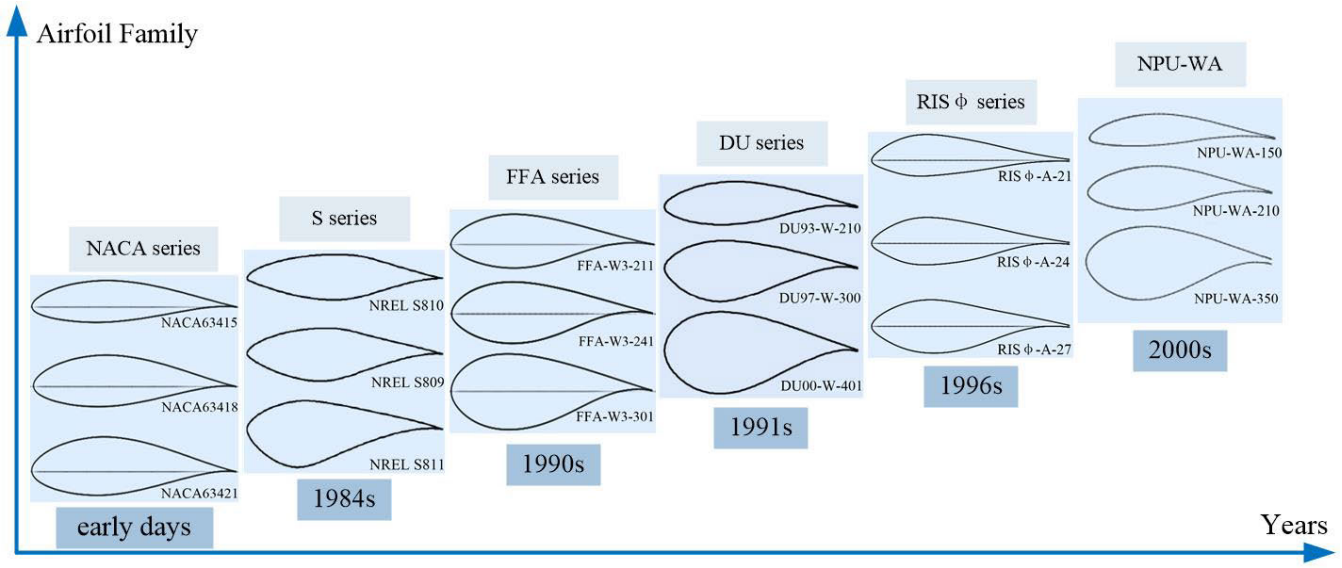

FIGURE 1. Research and development history of the wind turbine blade airfoil family.

wind turbines, and there is still room for improvement in the development of airfoil families as the understanding of wind turbine systems deepens.

Wind turbine blade shape is obtained by stacking multiple airfoils, and airfoil according to the relative thickness of the different divided into the blade tip airfoil (the portion beyond 80% of the blade spanwise position), the mid-blade airfoil (the portion between 30%-80% of the blade spanwise position), the blade root airfoil (the portion within 30% of the blade spanwise position), which, the blade tip airfoil maximum relative thickness is generally not more than 21%, the mid-blade airfoil maximum relative thickness in 21%-28% between, the blade root airfoil maximum relative thickness is above 28%. The portion of the wind turbine blade in the spanwise position of 70%-90% can capture more than 60% of the wind energy, therefore requires the blade tip airfoil to have a high maximum lift-to-drag ratio, a small running angle of attack, good stall characteristics and geometric compatibility. The blade root airfoil mainly takes into account the complex flow characteristics of large running angles of attack and easy separation and uses a relatively thicker airfoil to obtain greater structural rigidity and geometric volume, while requiring a high lift coefficient. The mid-blade airfoil needs to integrate the design requirements of the blade tip and root airfoil, and should have a relatively high maximum lift coefficient so that the chord length of the blade can be reduced when designing the blade tip speed ratio, thus reducing the load on the blade during operation [10].

There are three main methods of developing airfoil families. The first is the positive design method, in which the aerodynamic characteristics of the airfoil are calculated based on existing airfoil data and the designer's experience, through continuous correction of the initial airfoil, combined with numerical simulations or wind tunnel test methods, and the target airfoil with the maximum lift coefficient or maximum lift-to-drag ratio is obtained empirically. The second is the inverse design method, which gives the ideal target pressure distribution (or velocity distribution) under the design state, and determines the corresponding airfoil geometry when the given flow field characteristics are satisfied by iterative calculation of the flow field. The third is the direct optimization method, which combines the airfoil flow field solution procedure with the optimization procedure to find the extreme value of the objective function under the constraints by perturbing the airfoil shape to obtain a new airfoil shape that satisfies the conditions. In the optimization process, the optimization algorithm has a crucial influence on the final design result. Gradient-based algorithms (finite difference methods, local linearization methods, adjoint methods, etc.) have fast search speed, but the solution searched for maybe a local extreme value rather than an optimum value. Random class algorithms (genetic algorithms, simulated annealing algorithms, ant algorithms, particle swarm algorithms, etc.) have a long search time but introduce random parameters in the search for the optimal solution, which can break out of the local extreme value trap and are global optimization algorithms. In contrast, the optimization algorithms must be based on high-confidence estimates of aerodynamic characteristics, mainly CFD, XFOIL, artificial neural networks, deep learning, agent models (Kriging model, response surface model, POD model), etc. The main contents of the existing literature for airfoil optimization design are shown in Table 1 of the Appendix.

Tang et al. [11] used the control coefficients of the Hicks-Henne parametric method as design variables, the maximum mean lift-to-drag ratio and the minimum fluctuation range of the lift-to-drag ratio as objective functions, genetic algorithm and Kriging model were used to establish

an airfoil optimization model for the S809, and it was found that the range of the standard deviation fluctuation of the lift-to-drag ratio of the optimal airfoil was reduced by 17.96%, and the mean lift-to-drag ratio did not decrease.

Saleem and Kim [12] used 12 geometrical parameters of the NACA-9415 as design variables to control the shape of the airfoil. The objective function was designed to maximize the airfoil lift coefficient, optimization was performed using a single-objective genetic algorithm developed in MATLAB, and aerodynamic analyses were also carried out by using the XFOIL code, and saved aerodynamic characteristics including lift coefficients, drag coefficients and pressure coefficients for the evaluation of the fitness function in the optimization algorithm. The results showed that the angle of attack was 0°, the optimized airfoil increased the lift coefficient by 18%, and the lift-to-drag ratio increased by 34% compared to the NACA-9415 airfoil.

Ram et al. [13] used the composite Bessel curve to define the geometry of the airfoil, considered the geometrical constraints of the airfoil to maximize the lift-to-drag ratio as the objective function, and used a genetic algorithm to optimize the airfoil USP07-45XX. After optimization, the lift coefficient of the airfoil USP07-4510 showed little variation under both smooth and rough conditions, with lift-to-drag ratios that were all superior to those of SG6043.

Li et al. [14] proposed an aerodynamic design concept to meet the requirements of ''high efficiency, low ultimate load, stability, and wide operating range'' of the blade, and established an integrated optimization platform for the overall design of thick airfoils by combining the genetic algorithm and the Isight, adopted the B spline curve to describe the geometry of the airfoil DU97-W-300, and carried out the aerodynamic performance calculations based on the RFOIL, and the new airfoil obtained finally had a high design coefficient of lift, an acceptable maximum lift-to-drag ratio, a moderate stall parameter, and a desirable stability parameter.

Ribeiro et al. [15] combined genetic algorithm and ANN to optimize the airfoil GA(W)-1 with the maximum lift-to-drag ratio as the objective function, constrained the maximum thickness and minimum thickness of the airfoil, and used CFD method for the flow field analysis to establish the airfoil optimization model, and the optimized airfoil lift-to-drag ratio was about 100, and artificial neural network was able to model the airfoils with large attack angles and reduced the computation time by nearly 50%.

Wang et al. [16] used airfoil functional integral theory to describe the geometry of the airfoil, maximized the lift-to-drag ratio under smooth and rough conditions at multi-point angles of attack as the objective function, used PSO optimization algorithm to calculate the aerodynamic performance of the airfoil with the help of RFOIL software, and carried out the optimal design of the airfoil WQ-A. The optimized WQ-A B210 airfoil exhibited a better average lift-to-drag ratio in the range of 2° ∼12° attack angle, which was improved by about 6.25%.

Kaviani and Mohammad [17] used PSO optimization algorithm to optimize the airfoil S818, S825 and S826, described the airfoil geometry with CST parameterization method, maximized blade power generation, constrained the relative thickness conditions of airfoil, and the optimized airfoil increased the power generation of wind turbines by 2.68%.

Ju et al. [18] combined airfoil functional integral theory and the Hicks-Henne method and used PSO algorithm to establish optimization models for the airfoil Risø-A1-15 by taking the linear weighted sum of maximum values of lift-to-drag ratios at different angles of attack as the objective, and the first 10 coefficients as the design variables. The results showed that the new airfoil's lift coefficients were improved by an average of 38.62% and 6.48%, and the maximum lift-to-drag ratio was improved by 6.02% and 1.75%, respectively.

Chen et al. [19] combined the improved particle swarm algorithm and the parametric expression method of the airfoil based on the general integration theory to establish an optimization model taking into account the aerodynamic performance and static aeroelasticity, and took NACA 64618 as the initial airfoil, calculated the aerodynamic performance of the airfoil by RFOIL, and the new airfoil finally obtained was conducive to reducing the torsional displacement of the blade tip and improving the ability of suppressing the torsional dispersion of the blade.

Liu et al. [20] combined GA and SA algorithms to optimize the design of the airfoil NACA4418 with the maximum lift-to-drag ratio as the objective function, constraining the airfoil thickness variation within 5%, and the maximum thickness is located at the position of 0.24∼0.35 of the chord length. The airfoil optimized by the improved simulated annealing genetic algorithm showed a 21.97% increase in lift-to-drag ratio and a more uniform pressure distribution.

Wen [21] used a Bezier polynomial to simplify the airfoil curve into eight pairs of coordinates and used a GABP artificial neural network to optimize the design of the S809 airfoil. The method used 1446 sets of data as the training set and 50 sets of data as the test set. The prediction results of the artificial neural network for the maximum lift-to-drag ratio and the maximum lift coefficient were both 90% accurate. The drag coefficient of the optimized airfoil was unstable, the lift coefficient was better and the maximum lift-to-drag ratio of the airfoil was significantly better than that of the original airfoil.

Wei et al. [22] selected the coordinates of eight Bezier curve control points as design variables, and used the lift-to-drag ratio increment and variance as optimization objectives. NSGA II was used to optimize low Reynolds number airfoil E387 by direct search method. After optimization, the lift-to-drag ratio variance of the airfoil was smaller, and the airfoil was increased evenly at different angles of attack, while maintaining similar characteristics to the original airfoil.

Vecchia et al. [23] combined Nash equilibria (NE), genetic algorithms (GA), PARSEC and Games Theory to establish an airfoil optimized design model, using XFOIL as an external aerodynamic solver, and applying a fixed transition at 5% of the chord length on the upper and lower sides of the S809 airfoil. Starting from the original airfoil coordinates, the optimization process was run with a range of PARSEC parameters varying by 10% relative to the starting parameters, without any geometrical or aerodynamic constraints, resulted in an increase in airfoil thickness and curvature and an increase in lift coefficient.

Lee and Kwon [24] used Latin hypercube sampling to randomly select a set of design variables within a given range, the Hicks-Henne shape function was used to determine the designed blade spanwise cross-sectional profile, and applied coupled CFD-CSD methods and the optimization methods based on ANN and GA to find the optimum blade shape. This optimization resulted in a 0.82% reduction in the energy cost of the NREL VI rotor blade after optimization, and the energy cost of NREL 5 MW wind turbine blades was reduced by 1%.

Zhang et al. [25] used a fourth-order polynomial function to describe the airfoil profile and used the lift force calculated by the Kuta-Jukovsky (KJ) theorem as the objective function to optimize the NACA4412 airfoil profile using the cuckoo search algorithm (CSA). The results showed that the average lift-to-drag ratio coefficient and the maximum lift-to-drag ratio coefficient of the CSA-KJ4412 airfoil increased, and the average lift-to-drag ratio improved by 4.53% compared to NACA4412.

Akram [26] developed an integrated code based on a genetic algorithm to optimize the asymmetric NREL S809 airfoil by using the Class Shape Transformation (CST) and PARSEC parameterization methods to analyze its aerodynamic characteristics and maximize the lift of the airfoil. The results show that the CST-optimized airfoil improves the lift coefficient by 11.8% and the lift-to-drag ratio by 9.6%, while the PARSEC-optimized airfoil improves the lift coefficient by 10% and reduces the lift-to-drag ratio by 2%.

Oh [27] described the geometric shape of the airfoil DU21-A17 based on a parametric approach of Bezier curves, used the polynomial response surface method (RSM) and artificial neural networks (ANN) to construct an alternative model with the maximization of the lift-to-drag ratio as the objective function, and used a genetic algorithm to optimize the design. The results showed that when the provided dataset had high complexity, the ANN-calculated proxy model has high prediction accuracy, but when the dataset has low complexity, the accuracy of the RSM decreases.

Benim et al. [28] combined computational fluid dynamics (CFD) analysis with response surface methodology (RSM), bi-objective mesh adaptive direct search (BiMADS) optimization algorithms, and automated geometry and mesh generation tools to develop an automated two-dimensional airfoil shape optimization procedure for small horizontal axis wind turbine (SHAWT) and showed that high thrust and aerodynamic stability performance improvements can be achieved by modifying the blade shape.

Miller et al. [29] used Bezier curves and XFOIL software to design a flat-backed airfoil family, and the new airfoil CU-W1-XX family, provided equal or better performance than other airfoils.

Ju et al. [30] based on the small sample neural network applied particle swarm optimization algorithm to establish an airfoil aerodynamic performance optimization design model for NACA4415 airfoil under multiple constraints. The results showed that the new airfoil improved the maximum lift coefficient by 6.96% and the maximum lift-to-drag ratio by 7.37% within the range of main running angle of attack.

In addition, many other researchers consider the effects of noise, turbulence, stiffness, roughness and other factors to optimize the design of wind turbine airfoils from different perspectives. In this paper, a single-objective optimization design method for airfoil families is established considering different angles of attack, different Reynolds numbers and different weight coefficients, and finally, the new airfoil family with high performance is obtained. Through analysis and discussion of the optimization results, the rationality and effectiveness of the optimization method are verified, to broaden the ideas for the design of special airfoil families for wind turbines.

The main contributions of this paper are: (1) Establishing a single-objective optimization mathematical model for high-performance wind turbine blade airfoil families, and obtaining seven groups of airfoil families (ZDGN-ASG, ZDGN-ASP, ZDGN-ASPG, ZDGN-ASR1, ZDGN-ASR5, ZDGN-ASQ3, and ZDGN-ASQ8), whose lift coefficients and lift-to-drag ratios are superior to those of conventional families under both design and non-design conditions. (2) The new airfoil family has widened the region of the high lift-to-drag ratio at most angles of attack, especially at the design angle of attack. The distribution of pressure coefficients is improved with the increase of Reynolds number, and the pressure changes are smoother. The maximum lift coefficients and lift-to-drag ratios of the new airfoil family are better than those of the conventional families under different weight coefficients. (3) Applying the new airfoil family to the actual 1.2 MW blade, the output power obtained from the new blade in the range of wind speed 8∼11 m/s and the wind energy utilization factor obtained from the range of tip speed ratio 5∼7 are significantly improved compared with the initial blade.

This paper is organized as follows: Section II introduces the aerodynamic performance calculation method, Section III describes the airfoil parametric modeling method and verifies the feasibility of the method, Section IV introduces three single-objective optimization algorithms, Section V establishes the mathematical model for airfoil family optimization, the optimization results are analyzed and discussed in Section VI, the results of actual blade performance are

verified in Section VII, and conclusions and prospect are given in Section VIII.

II. AERODYNAMIC PERFORMANCE CALCULATION METHOD

Accurate and efficient calculation methods for airfoil aerodynamic performance are a necessary prerequisite for the optimal design of wind turbine airfoils. The main calculation methods are based on the panel method for the uncompressible potential flow equation and the boundary layer equation, computational fluid mechanics method based on Reynolds mean NS equation and wind tunnel experiment method. The CFD method is costly and time-consuming, and the method of establishing a turbulence model and judging the transition is incomplete, which limits the application of this method in the optimization design of airfoils that require iterative calculation. Although accurate experimental data can be obtained from wind tunnel experiments, they are limited by the experimental conditions, and the experimental period is long and expensive. The method based on the panel method of solving the completely incompressible potential flow equation coupled with the boundary layer integral equation is widely used in the iterative design of wind turbine airfoils, as it ensures a rapid and robust solution, while taking into account the presence of a viscous boundary layer to make the calculation results accurate and reliable.

The basic principle of the panel method is to lay out the surface source intensity distribution or surface vortex intensity distribution on the airfoil surface and superimpose it on the straight uniform flow to solve for the flow field. The process is to divide the airfoil surface into a sufficient number of finite panels, arrange the surface sources or surface vortices on each panel, establish a linear system of equations satisfying the no-penetration boundary conditions and the airfoil trailing edge Kutta condition at the control points on each panel, and finally solve the system of equations to determine the panel strength and obtain the disturbance velocity potential to further calculate the airfoil surface pressure distribution, lift drag and moment. The XFOIL program based on the panel method is used to calculate the aerodynamic parameters of the airfoil. It is characterized by its high computational efficiency, short computing time and high accuracy of the results. The reliability of the XFOIL program has been verified by a large number of tests, and it can be seen from the literature [31] that the computational results of the XFOIL code are in good agreement with the experimental values. Therefore, the XFOIL calculation program is used in this paper for the optimal design of the airfoil.

III. PARAMETRIC MODELING METHOD

The airfoil parameterization is the basis for the optimal design of wind turbine airfoils, which determines the size and complexity of the design variable space and is used throughout the whole optimization design process, having a significant impact on the optimization results and efficiency. The airfoil geometry is generally represented in the form of discrete coordinate points, and the use of airfoil coordinate points as design variables in the optimization process will make the optimization process cumbersome and difficult to converge. Therefore, when optimizing the design of the airfoil, a reasonable parametric method should have the controllability and completeness to accurately and flexibly describe the geometry of the airfoil with as few characteristic parameters as possible, while controlling the overall trend and local variations of the geometry through the characteristic parameters.

There are various ways to parametrize express the airfoil according to different mathematical models, and the commonly used parametric methods are the shape function perturbation method (polynomial shape function, Hicks-Henne shape function), control point method (Bezier function, B-spline function), composite mapping method (shape function), etc. Among them, the Hicks-Henne shape function perturbation method has the advantages of smooth airfoil shape, fewer design variables, less oscillation, accuracy and stability, It's widely used in the field of airfoil optimization design. The basic principle is to superimpose the perturbation terms of thickness and curvature onto the base airfoil to achieve the expression form of the new airfoil, while the standard Hicks-Henne shape function has poor control over the trailing edge of the airfoil, limiting the sample space of the airfoil in the optimization design process. This paper, therefore, uses an improved Hicks-Henne shape function to characterize the airfoil in the form of a new trailing edge shape function added to the original shape function to improve the problem of insufficient trailing edge perturbation. The calculation formula of the improved Hicks-Henne type function is:

$$y_u = y_{o\_u} + \sum_{k=1}^{k=n} c_k f_k(x) \tag{1}$$

$$y_l = y_{o\_l} + \sum_{k=1}^{k=n} c_k f_k(x) \tag{2}$$

$$f_k(x) = \begin{cases} x^{0.25}(1-x)e^{-20x} k = 1 \\ \sin^3(\pi x^{e(k)}) 1 < k < n \\ \alpha x(1-x)e^{-\beta(1-x)} k = n \end{cases} \tag{3}$$

$$e(k) = \ln 0.5 / \ln x_k \; 0 < x_k < 1 \tag{4}$$

In the equation, x is the chord coordinates of the airfoil;y_{o_u} and y_u are the vertical coordinates of the upper profile of the base airfoil and the design airfoil respectively;y_{o_l} and y_l are the vertical coordinates of the lower profile of the base airfoil and design airfoil respectively; c_k is the control coefficient for the shape function $f_k(x)$, which is also the design variable for the geometry of the airfoil, and its range of values determines the size of the airfoil design space. x_k is the design node and α is the value of the change in the control slope, generally take $\alpha \in [5, 15]$. β is the control decay rate coefficient. In this paper, we use the reference value $\alpha = 8\beta = 10$ given in the literature [32].

As the airfoil shape parameterization has an important influence on the convergence of the optimization solution, it needs to be checked analytically by geometric convergence and aerodynamic convergence. A comparison of the Hicks-Henne shape function parameterization method with the initial airfoil shapes NACA63418, NACA63427 and NACA63436 is shown in Fig. 2 to analyze the residuals of the airfoil shape fit at different orders, where x/c ranges from -1 to 0 for the top surface of the airfoil and from 0 to 1 for the bottom surface of the airfoil, and the smaller the value of the upper and lower airfoil fit residuals, the more the fitted airfoil shape closer to the initial airfoil shape. As can be seen from the graphs, the fitted residuals are less than 2e-3 at the 7th, 7th and 6th orders respectively, and the parameterized airfoils are essentially the same as the initial airfoil, indicating that the Hicks-Henne shape function parameterization method is highly reliable in describing the airfoil geometry. Further analysis of the aerodynamic convergence characteristics of the airfoil, using the XFOIL program to calculate the pressure distribution of the fitted airfoil and the initial airfoil, the pressure distribution trends for the angles of attack of 5°, 6° and 7° respectively match very closely with the initial airfoil, indicating that the fitted airfoil can be used instead of the initial airfoil to analyze the aerodynamic characteristics. The control coefficients obtained by applying this parameterization method to the remaining NACA634XX series airfoils are shown in Table 1.

IV. SINGLE OBJECTIVE OPTIMIZATION ALGORITHM

A. GENETIC ALGORITHM

Genetic algorithm (GA) [33] is an efficient, parallel, global search modern optimization method combining Darwinian evolution and Mendelian genetics. The principle is based on a coding mechanism, which starts from a randomly generated initial population, simulates natural selection and heredity in which the phenomenon such as replication, crossover and mutation occur, and follows the principle of survival of the fittest, gradually generating a near-optimal solution in the potential solution population, thereby evolving the population and eventually obtaining the optimal individual. The advantages of this method are its simplicity, generality, robustness, and no strict requirements on the search space in the optimization process. It can quickly find the optimal solution in a large and complex search space and avoid falling into a local optimum and has been used in wind turbine airfoil optimization design problems maturely.

The basic process of a genetic algorithm is broadly divided into several steps: determining the basic parameters, developing a coding scheme, generating an initial population, determining the fitness function, performing genetic operations, generating a new population, and stopping iteration when the conditions are met. The optimization process of a genetic algorithm is shown in Fig. 3, where selection, crossover and mutation are the three core operations of a genetic algorithm. The selection operation is to select good individuals with high fitness and eliminate poor individuals with low fitness in each generation; the crossover operation is to obtain new individuals by exchanging some genes of two parent individuals, which can improve the global search ability of the genetic algorithm; the mutation operation is to change some gene loci on the chromosome of individuals, which can improve the diversity of individuals in the population to a certain extent. The control parameters of the genetic algorithm affect the accuracy and efficiency of the optimization process, and suitable parameters need to be selected for the solution. In this paper, the genetic algorithm is optimized with a population size of 50, a crossover probability of 0.5, a mutation probability of 0.5 and a maximum evolutionary generation of 200, while other parameters are set by default.

B. PARTICLE SWARM OPTIMIZATION ALGORITHM

The particle swarm optimization (PSO) algorithm [34] is an intelligent evolutionary algorithm that simulates the movement behavior of a flock of birds gathering, migrating and foraging to find food through the sharing of position and velocity information between individuals. The flock of birds is abstracted as a swarm of particles without mass and volume, with velocity representing how fast the particles move and position representing the direction in which they move. The finite number of possible solutions to the optimization problem is initialized as a swarm of particles, each particle judges the current position of its virtues or defect degree based on the fitness function in the algorithm, and compares it with the virtues or defect degree of the historical optimal position to find the current individual extreme value, and then shares the individual extreme value with the other particles in the whole swarm, taking the optimal individual extreme value as the current global extreme value of the whole swarm. All particles in the swarm adjust their velocity and position according to the current individual extreme value they find and the current global extreme value shared by the whole swarm, so that the algorithm moves on to the next iteration. When the individual fitness of the particles within the swarm does not change significantly or the optimal particle position in the solution space is found, the whole swarm stops iterating and outputs the optimal position of the entire swarm, i.e. the optimal solution to the optimization problem.

The optimization process of the particle swarm algorithm is shown in Fig. 4. The core step is to updating the position and velocity of each particle in the population, and the velocity update is the core of the core. The velocity of a particle is divided into a weighted vector sum of velocities in three directions: inertia-holding part, self-aware part, and social-aware part. The inertia-holding part represents the inertial flight of the particle along the current velocity and direction, belonging to the previous velocity of the particle; the self-aware part represents the particle's own thinking and is the distance between the particle's current position and its own best position; the social-aware part represents information sharing and cooperation between particles and is the distance between the particle's current position and the

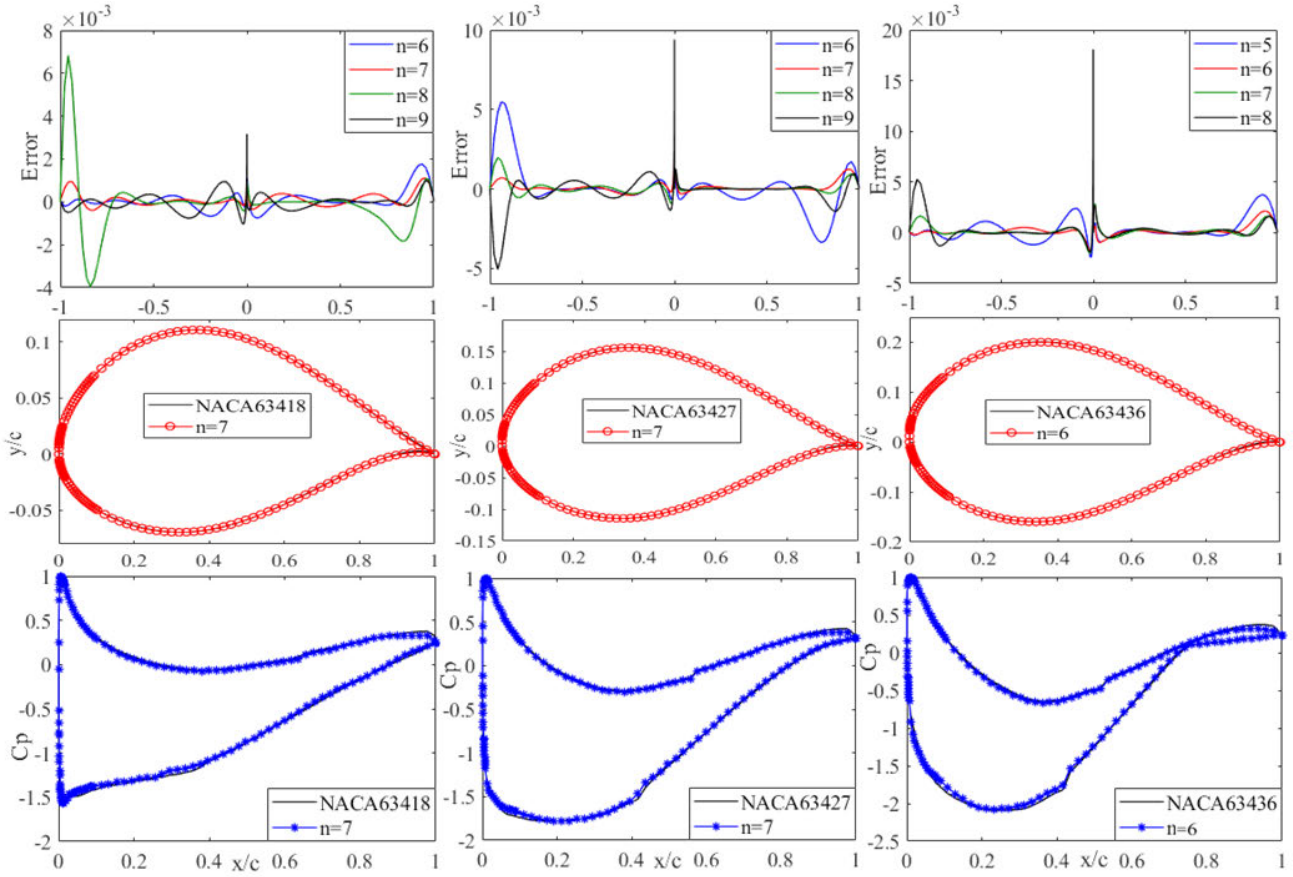

FIGURE 2. Comparison of parametric airfoil shape and initial airfoil shape.

TABLE 1. NACA634XX series airfoil parameterized control coefficient values.

Airfoil	Control Coefficient Values (e^{-3})													
	C1	C2	C3	C4	C5	C6	C7	C8	C9	C10	C11	C12	C13	C14
NACA63412	11	10.5	6.8	8.1	6.6	2.1	17.2	-1.5	-1.4	-0.5	2.7	1.3	3.6	3.8
NACA63415	16.3	13.5	8.5	9.8	7.7	3.6	12.7	-3.6	-4.2	-1.6	-0.8	1.5	2.1	5.9
NACA63418	18	13.6	8.1	10.4	7.4	4.9	8.7	-1.8	-4.1	-1.9	-0.3	1	2.6	4.6
NACA63421	25.4	16.3	10.5	11.2	9.1	3.9	13.9	0.1	-6.9	-3.7	-2.4	0.4	1.9	8.7
NACA63424	28.5	16.3	10.6	11.1	9.2	3.7	14.7	0.6	-7.3	-2.1	-4.1	1.4	0.8	8.5
NACA63427	25.3	13	10.2	7.9	8.9	3.8	10.7	3.3	-3.5	-1.6	-1.4	2.3	2.1	4.3
NACA63430	29.9	13.7	6.7	10.4	3.7	16.9	9.4	-0.5	-0.4	3	2.2	11.2	-	-
NACA63433	38.6	17.1	8.7	12.4	4.4	15.7	9.9	-4.1	-2	1.2	1.8	10.7	-	-
NACA63436	43.1	17.6	7.7	12.5	4.7	15.1	12.5	-3.2	-2.9	1.5	3.2	1.2	-	-

group's best position. The advantage of the particle swarm algorithm is that the principle is simple, easy to implement, fewer parameters need to be adjusted and convergence is faster. In this paper, the number of particles is 25, the inertia weight is 0.75, the acceleration factor is c1=c2=2, the maximum number of iterations is 150, the accuracy error of the optimal solution is 1e-6, and the other parameters are set by default.

C. PARTICLE SWARM OPTIMIZATION AND GENETIC ALGORITHM

The selection, crossover and mutation operations in the genetic algorithm allow the algorithm to have a wide search space and a strong global search capability in the optimization iteration process, but the convergence speed is slow. The particle swarm algorithm, by sharing information between particles, makes the algorithm converge fast but easily fall into local optimum. For this reason, the selection, crossover and mutation operations of the genetic algorithm are embedded in the particle swarm algorithm to form the particle swarm optimization and genetic algorithm (PSOGA) [35], which can maintain the information exchange between particles and the population diversity, avoid falling into the local optimum and improve the search efficiency of the algorithm.

The main difference of the PSOGA algorithm is that after the first velocity and position update of the swarm particles, the updated particles are evaluated again using the fitness function, based on which the swarm particles are selected

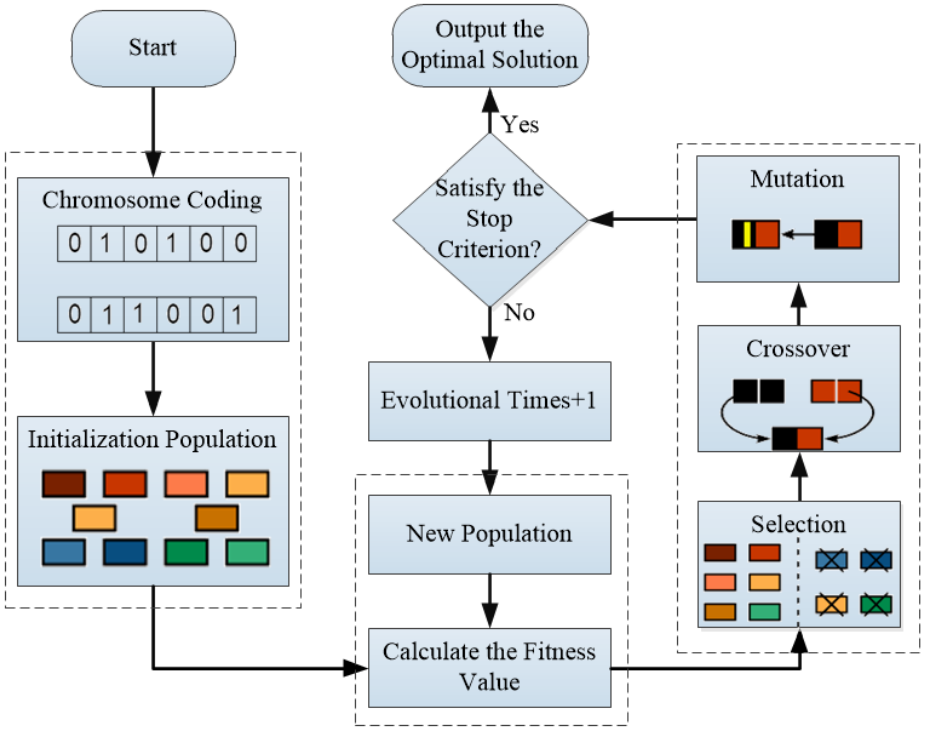

FIGURE 3. Genetic algorithm optimization process.

using the ranking method. After that, the velocity and position of the particles are crossed and mutated to produce a new generation of particles, and then the particles in the swarm move on to the next iteration by tracking the new individual and global extremes, and so on until the particles in the swarm find the optimal solution. The optimization process of the particle swarm genetic algorithm is shown in Fig.5.The parameters of the particle swarm genetic algorithm can be set according to the principles of the above two algorithms.

D. REASONS FOR CHOOSING THE OPTIMIZATION ALGORITHM

When choosing an optimization algorithm, some of the more common and classic algorithms, such as genetic algorithms, particle swarm algorithms, and their combinations, are selected because they possess specific advantages and applicability that make them well-suited to addressing a wide range of problems. The use of three different optimization algorithms allows for a more comprehensive demonstration of the characteristics and applied range of the various algorithms and allows for a comparison of their performance and effectiveness in solving problems.

Genetic algorithm is an optimization algorithm based on the principle of biological evolution, that searches for the global optimal solution or near-optimal solution by simulating the hereditary and mutation process in nature, it is less sensitive to the selection of initial parameters, has parallelism, and can process multiple solutions at the same time, improving the optimization efficiency. It is not restricted by the structure of the problem and shows a good performance in solving the complex and nonlinear optimization problems. It has been widely applied in practical applications such as model parameter optimization in machine learning and design optimization in the engineering field.

Particle swarm algorithm is an optimization algorithm based on group intelligence that searches for the optimal solution by simulating the particle's movement and communication with each other in the search space. Its advantage lies in the fact that it can converge to the local optimal solution faster, and it also has a certain global search ability, which is advantageous in dealing with high-dimensional, complex and nonlinear optimization problems. It is simple and easy to implement and has fewer adjustments of parameters. It is suitable for continuous optimization problems with constraints or multi-peak functions, and is widely used in different fields such as function optimization, production scheduling, neural network and decision tree training optimization, etc.

Particle swarm genetic algorithm is an optimization algorithm that combines natural evolution and group intelligence, which has both the global search ability of genetic algorithm and the local fine search ability of particle swarm optimization algorithm. This algorithm can not only enhance the coverage of the search space but also deal with large-scale, high-dimensional optimization problems more efficiently and quickly find the global optimal solution when dealing with the problem with multiple local optimal solutions. The search process is relatively stable. It has been widely used in many

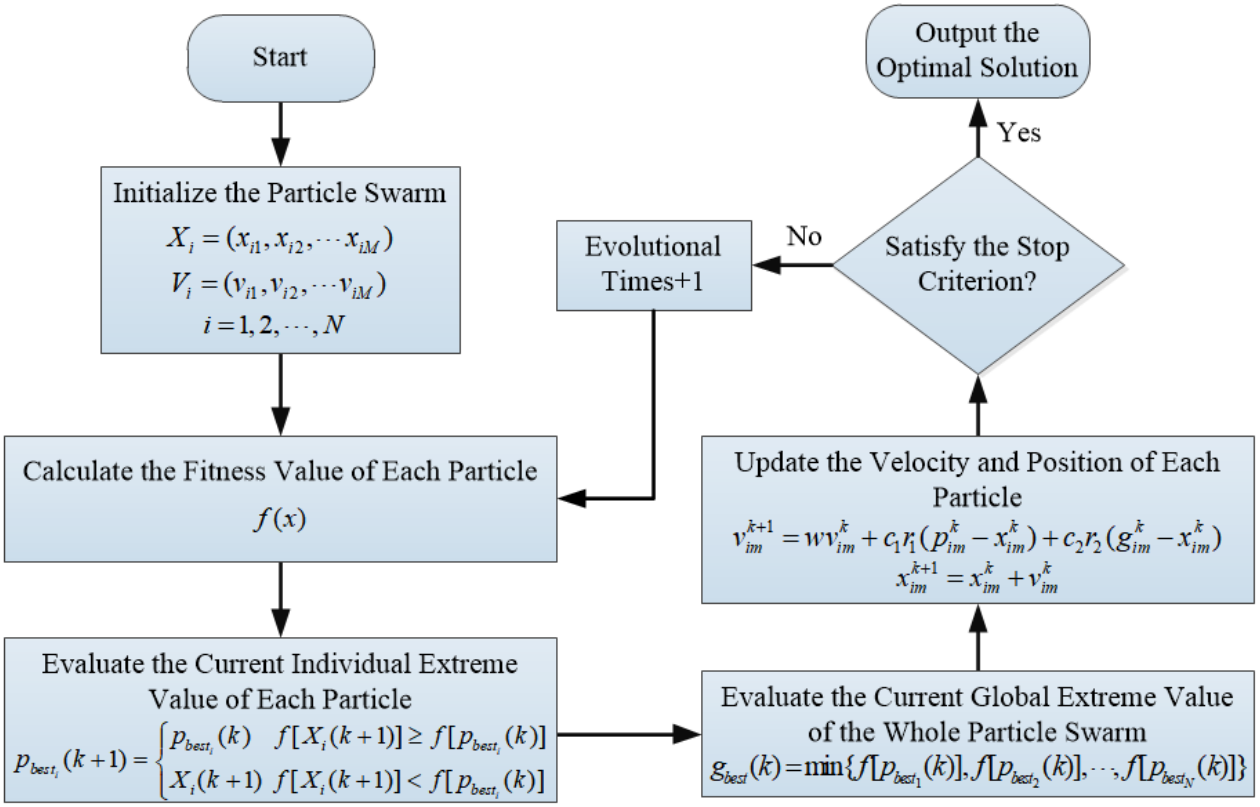

FIGURE 4. Particle swarm optimization algorithm process.

application areas, such as power system optimization, path planning, deep learning, etc.

In this paper, the aforementioned three optimization algorithms are chosen because of the simplicity and easy understanding of the algorithms, which can conveniently implement parallel computing and make them more efficient in dealing with large-scale and complex problems, and their effectiveness and reliability have been verified in many practical application scenarios, and they have certain versatility and adaptability. However, with the continuous development of technology, new optimization algorithms are emerging, such as simulated annealing algorithms, ant algorithms, etc., which may require more in-depth research and understanding, as well as more parameter adjustments and finer settings, which may increase the difficulty and complexity in use, and thus may not be preferred choice.

V. MATHEMATICAL MODEL FOR AIRFOIL FAMILY OPTIMIZATION

1) Objective function In this paper, the maximum lift-to-drag ratio and lift coefficient of the wind turbine airfoil are taken as the multi-objective optimization function, the weight coefficient method is adopted, and the weight coefficient of optimization variables is set as 0.5. Since the numerical difference between the lift coefficient and lift-drag ratio is nearly two orders of magnitude, 0.01 times the lift-drag ratio and lift coefficient are taken as the optimization objectives, and the multi-objective optimization solution is effectively transformed into a single-objective solution problem. With reference to the operating conditions of horizontal axis wind turbine blades, the design Reynolds number of the airfoil is finally determined to be 3e6. According to the design requirements of the blade airfoil, the attack angle of the blade tip airfoil is determined to be 2°, the attack angle of the mid-blade airfoil is determined to be 5°, and the attack angle of the blade root airfoil is determined to be 10°. The objective function is expressed as:

$$f(x) = q_1 \times 0.01 \max(Cl/Cd) + q_2 \max(Cl) \quad (5)$$

where q1 and q2 are the weighting coefficients and are taken as 0.5 respectively.

2) Design variables
The improved Hicks-Henne shape function control coefficient is used as the design variable, and the airfoil parameterization calculation program is written based on MATLAB. Usually, the number of design variables increases in the process of parametric modeling and the ability to characterize the airfoil profile is enhanced, but too many control variables will greatly increase the optimization time. Considering the influence of the

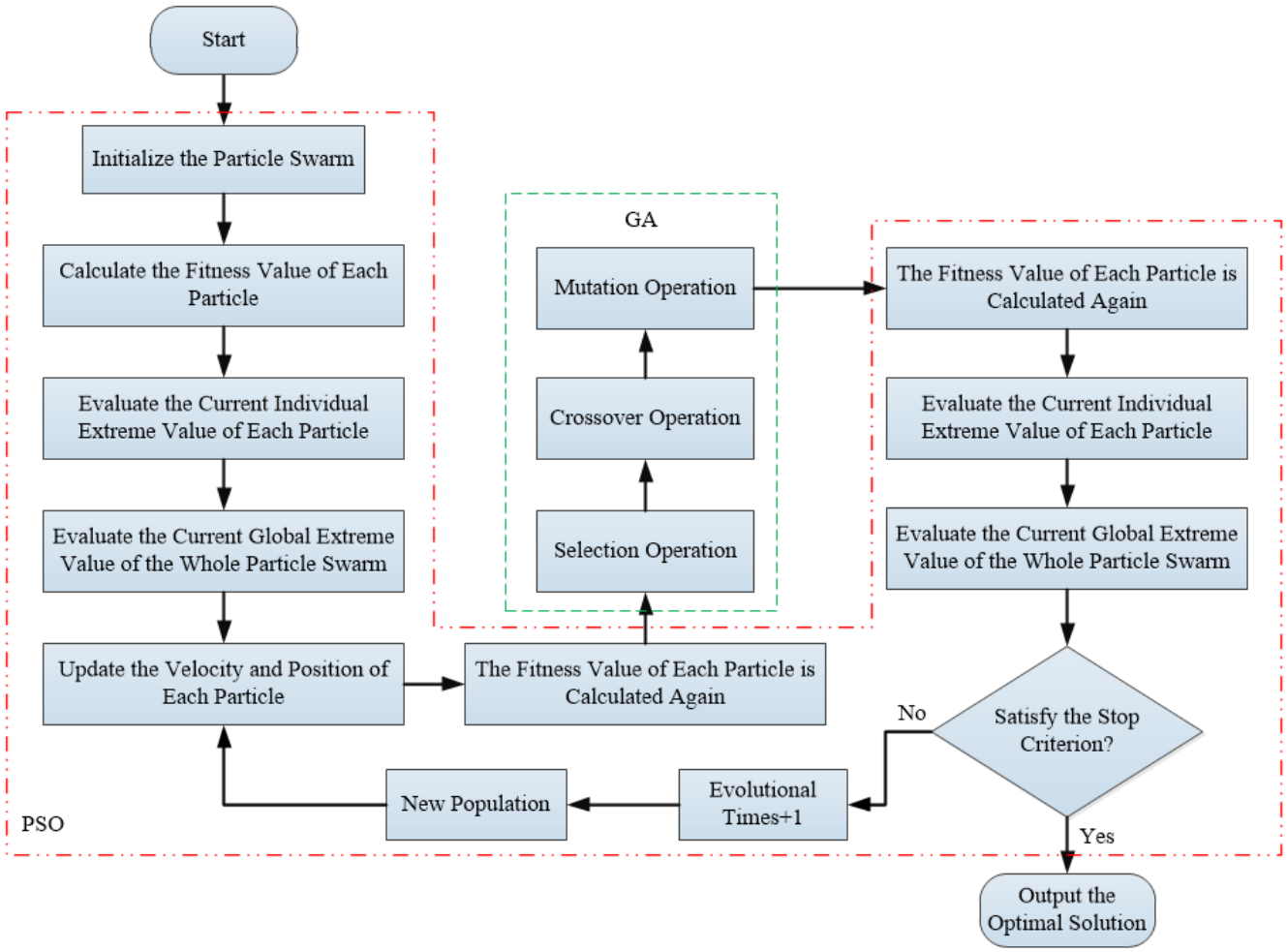

FIGURE 5. Particle swarm genetic algorithm optimization process.

control coefficient on the coverage characteristics of the airfoil design space and the freedom characteristics of the profile, 7 or 6 coefficients were selected from the upper and lower airfoil surfaces as the variables for optimal design:

$$c = [c_1, c_2, c_3, c_4, c_5, c_6, c_7, c_8, c_9, c_{10}, c_{11}, c_{12}, c_{13}, c_{14}] \quad (6)$$

where $c_1 \sim c_7$ is the upper airfoil control coefficients and $c_8 \sim c_{14}$ is the lower airfoil control coefficients.

3) Constraints

There are two types of airfoil optimization constraints: geometric constraints and aerodynamic performance constraints, the former mainly refers to the range of values of the relevant control parameters of the airfoil profile curve that can be modified during the parametric modeling of the airfoil; the latter refers to the aerodynamic performance related parameters of the airfoil, such as lift-to-drag ratio, lift coefficient, drag coefficient, etc., while the specific constraints need to be determined according to the actual requirements of the airfoil. The main geometrical constraints in the optimization design are the range of values of the design variables, and the aerodynamic performance constraints are reflected in the constraints on the initial airfoil lift coefficient and lift-to-drag ratio under the design angle of attack: i.e. $C_l > C_{l0}$;$C_l/C_d > C_{l0}/C_{d0}$, where C_{l0} and C_{l0}/C_{d0} are the lift coefficient and lift-to-drag ratio of the initial airfoil.

To avoid the appearance of control coefficients established by the improved Hicks-Henne shape function method that do not have the features to control the shape of the airfoil, the design variables are controlled within the range of [-0.005,0.005], as shown in Fig. 6. In addition to considering the aerodynamic constraints of the airfoil, the structural requirements should also be met, taking into account the torque characteristics of the wind turbine airfoil during actual operation and the mutual compatibility of the designed airfoil with other wind turbine airfoils, the maximum thickness of

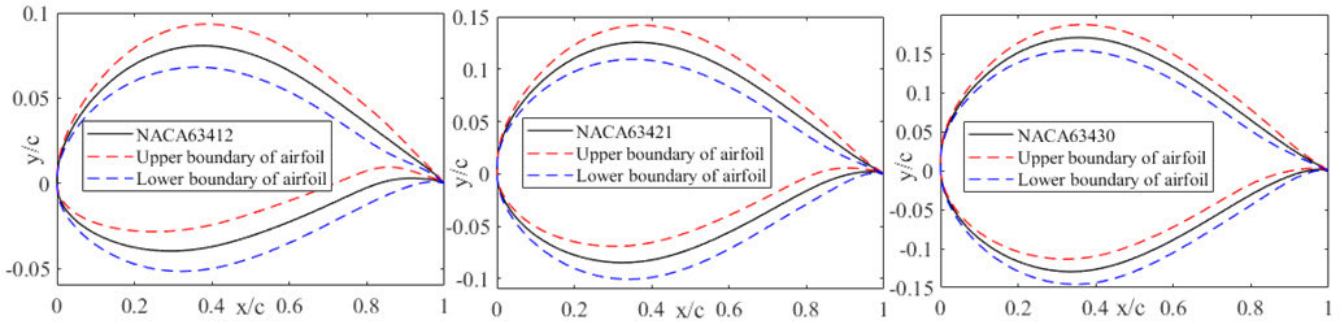

FIGURE 6. Airfoil design space.

the constraint is controlled within ±5% and the maximum thickness position is controlled between 25% and 40%.

VI. ANALYSIS AND DISCUSSIONS OF OPTIMIZATION RESULTS

A. ANALYSIS OF AIRFOIL FAMILY OPTIMIZATION RESULTS

Fig. 7 shows the geometric shape comparison of the NACA634XX series airfoil family after optimization by three algorithms. Compared with the initial airfoil, the optimized airfoil is more convex on the upper surface and more concave on the lower surface. Compared with the initial blade tip airfoil (NACA63412, NACA63415, NACA63418), after optimization, the leading edge of the blade tip airfoil remained unchanged within 0-0.02c, and the trailing edge of the airfoil changed greatly within 0.9c-1c. The thickness of the upper surface of the airfoil increased and the thickness of the lower surface decreased under the three optimization algorithms. Compared with the initial mid-blade airfoil (NACA63421, NACA63424, NACA63427), after optimization, the leading edge of the mid-blade airfoil remained unchanged within 0-0.05c, and the trailing edge of the airfoil changed little within 0.9c-1c. After optimizing NACA63421 by the PSOGA algorithm, the upper and lower surface thickness increases and decreases to the greatest extent, while after optimizing NACA63424 by the PSO algorithm, the upper and lower surface thickness increases and decreases to the greatest extent. Compared with the initial blade root airfoil (NACA63430, NACA63433, NACA63436), the leading edge and trailing edge of the blade root airfoil after optimization are unchanged, and the upper surface thickness of the optimization NACA63436 airfoil by the three algorithms changes little.

The new optimized airfoil is named ZDGN-ASY-XXXX, where Y represents the optimization algorithm, where G represents the genetic algorithm, P represents the particle swarm optimization algorithm, PG represents the particle swarm optimization and genetic algorithm, and XXXX represents maximum relative thickness of the airfoil. Table 2 shows the optimized airfoil family geometric characteristics and aerodynamic performance data. The geometric parameters include maximum relative thickness T_m, maximum thickness position x_{tm}, maximum curvature C_{am}, and maximum curvature position x_{cam}, and each parameter is a dimensionless quantity relative to the chord length c of the airfoil. The aerodynamic parameters include the lift coefficient, drag coefficient and lift-to-drag ratio coefficient at the design angle of attack. The maximum relative thickness of the new airfoil geometrical features ranges from 11.5%c to 36.5%c, with the maximum thickness position between 31%c and 36%c from the leading edge, the maximum curvature between 1.6%c and 3.6%c, and the maximum curvature position between 33%c and 58%c from the leading edge point.

The lift coefficient and lift-to-drag ratio of the three algorithms optimized airfoils are better than the initial airfoil. The PSO algorithm, PSOGA algorithm and PSO algorithm optimized airfoil have the largest lift-to-drag ratio at 2° angle of attack among the blade tip airfoils, with 8.942%, 17.925% and 23.287% improvements, respectively, when compared to the initial airfoil. The GA algorithm, PSOGA algorithm and PSO algorithm optimized airfoil have the largest lift coefficient at 2° angle of attack, with 11.774%, 23.389% and 28.665% improvements, respectively, when compared to the initial airfoil. The PSOGA algorithm, PSO algorithm and GA algorithm optimized airfoil have the largest lift-to-drag ratio at 5° angle of attack among the mid-blade airfoils, with 8.579%, 13.727% and 10.099% improvements, respectively, when compared to the initial airfoil. The PSOGA algorithm, PSO algorithm and PSOGA algorithm optimized airfoil have the largest lift coefficient at 5° angle of attack, with 8.438%, 15.674% and 8.820% improvements, respectively, when compared to the initial airfoil. The PSOGA algorithm optimized airfoil has the largest lift-to-drag ratio at 10° angle of attack among the blade root airfoils, with 17.949%, 18.507% and 10.491% improvements, respectively, when compared to the initial airfoil. The PSO algorithm, PSOGA algorithm and PSOGA algorithm optimized airfoil have the largest lift coefficient at 10° angle of attack, with 8.471%, 8.3% and 7.797% improvements, respectively, when compared to the initial airfoil.

B. OPTIMIZATIONS OF AIRFOIL SHAPE AT DIFFERENT ANGLES OF ATTACK

To ensured that the optimized new airfoil can achieve better performance over a wider operating range, the aerodynamic

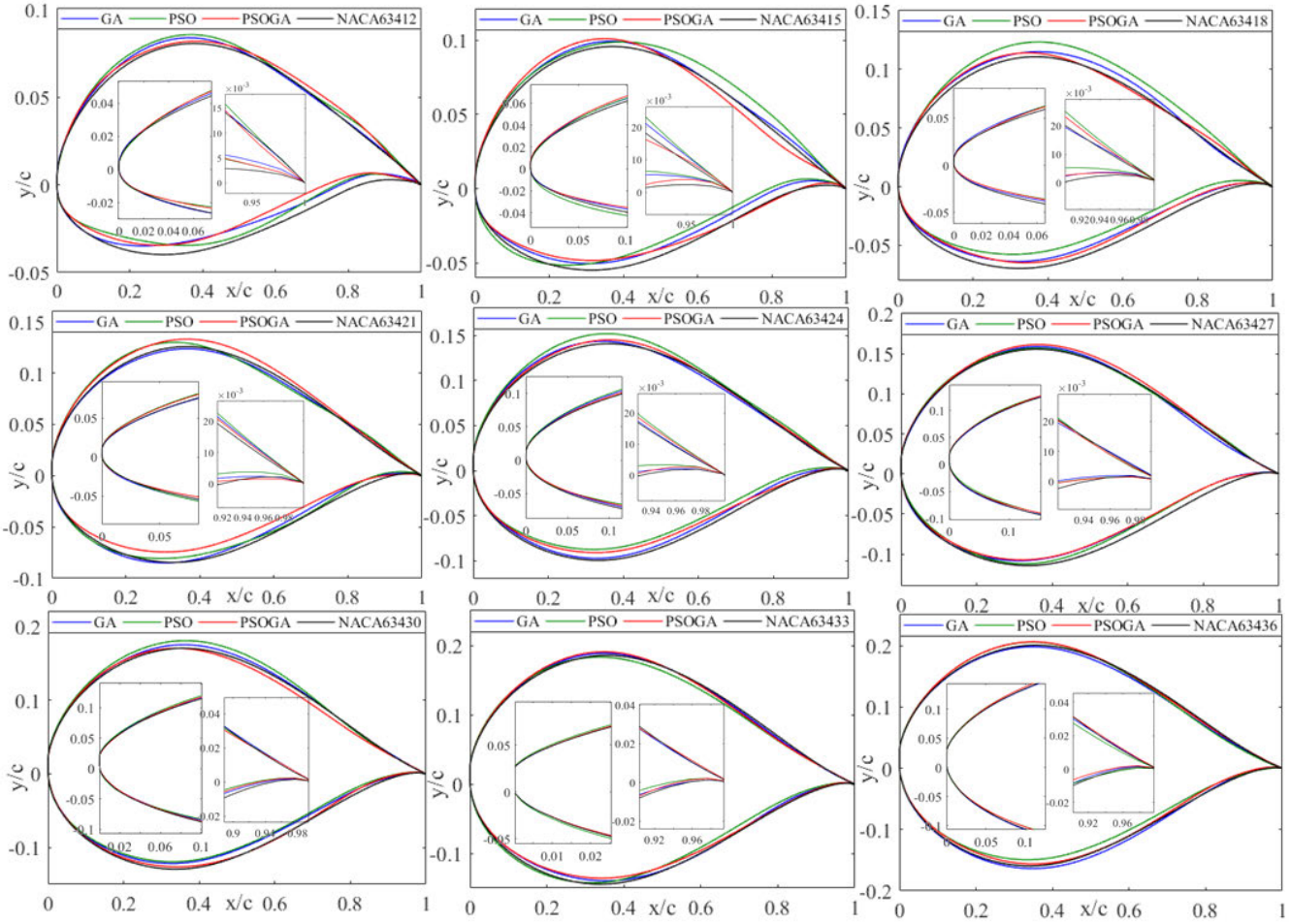

FIGURE 7. Comparison of airfoil geometry before and after optimization.

characteristics and pressure coefficients of the ZDGN-ASY-XXXX airfoil family and its respective corresponding initial airfoils were calculated and compared over the range of 0° ∼20° angles of attack, and the results are shown in Figs. 8∼10. The lift coefficients of the airfoils optimized by the three algorithms were improved at different angles of attack. The lift coefficients of the blade tip, blade middle and blade root airfoils are improved to a greater extent at angles of attack 0° ∼5°, 7° ∼12° and 13° ∼20° respectively, and the slope remains consistent in the attached flow region. At most angles of attack, especially the design angle of attack, the lift-to-drag ratio of the new airfoil family is higher than that of the initial airfoil, and the highest lift-to-drag ratio of the optimized airfoil is significantly increased, and the high lift-to-drag ratio region is widened, thus ensuring that the wind turbine blade still has good aerodynamic performance under non-design conditions and enabling the wind turbine to maintain a high power coefficient over a wide range of wind speeds.

Different airfoil geometry causes different surface pressure distributions, which affects its aerodynamic characteristics. The larger the area enclosed by the pressure coefficient curve, the greater the pressure difference between the upper and lower surfaces of the airfoil and the higher the lift of the airfoil. In the range of 0.5c-0.7c, the pressure on the lower surface of the new airfoil family is higher than that of the initial airfoil at the design angle of attack, while the pressure on the lower surface increases and the pressure on the upper surface decreases in the rest of the range, resulting in an increase in the lift coefficient, an increase in the lift-to-drag ratio and better aerodynamic performance. The maximum positive pressure coefficient values for both the initial and optimized airfoils are located at the leading edge of the airfoil and are around 1. The bottom end of the negative pressure coefficients for the blade tip, blade middle and blade root airfoils are around −1, −1.6 and −2.5 respectively. The optimized surface pressure coefficient curves of the blade tip airfoil are fuller than those of the initial airfoil, the upper and lower surfaces of the mid-blade airfoil have a smooth transition in pressure difference, and the upper surface of the blade root airfoil has too much curvature, resulting in a strong pressure shock wave at the back of 70% of the chord length.

TABLE 2. Optimized airfoil family geometric characteristics parameters and aerodynamic performance data.

Airfoil Family		T_m/%	x_{tm}/%	C_{am}/%	x_{cam}/%	C_l	C_d	C_l/C_d
the Blade Tip Airfoil	ZDGN-ASG-11.69	11.69	31.90	2.68	43.70	0.655	0.005	132.023
	ZDGN-ASG-14.89	14.89	33.90	2.59	45.70	0.622	0.005	125.688
	ZDGN-ASG-17.80	17.80	35.50	2.84	53.80	0.679	0.0053	127.273
	ZDGN-ASP-12.04	12.04	35.80	2.57	39.60	0.649	0.0047	136.983
	ZDGN-ASP-14.70	14.70	33.60	3.03	57.80	0.681	0.0052	131.139
	ZDGN-ASP-18.00	18.00	35.50	3.51	49.70	0.781	0.0056	138.974
	ZDGN-ASPG-11.51	11.51	33.70	2.76	55.80	0.651	0.005	131.402
	ZDGN-ASPG-14.91	14.91	33.60	2.67	37.60	0.728	0.0052	139.785
	ZDGN-ASPG-17.88	17.88	34.00	2.47	37.60	0.666	0.0057	117.107
the Mid-Blade Airfoil	ZDGN-ASG-20.78	20.78	33.60	2.27	53.80	0.988	0.0065	151.093
	ZDGN-ASG-24.06	24.06	33.50	2.36	43.60	0.999	0.007	142.923
	ZDGN-ASG-26.65	26.65	34.00	2.79	49.70	1.021	0.0071	143.394
	ZDGN-ASP-21.04	21.04	31.5	2.51	37.60	1.025	0.0066	154.99
	ZDGN-ASP-23.88	23.88	34.00	3.31	41.60	1.107	0.007	159.023
	ZDGN-ASP-26.88	26.88	34.00	2.52	53.80	0.999	0.0073	137.598
	ZDGN-ASPG-20.66	20.66	34.00	3.15	47.70	1.041	0.0066	158.880
	ZDGN-ASPG-23.54	23.54	35.50	2.83	45.70	1.025	0.0067	153.091
	ZDGN-ASPG-26.81	26.81	34.00	2.99	51.80	1.026	0.0073	139.713
the Blade Root Airfoil	ZDGN-ASG-29.68	29.68	34.10	2.86	47.70	1.424	0.0139	102.387
	ZDGN-ASG-32.84	32.84	35.40	2.46	33.40	1.327	0.0157	84.280
	ZDGN-ASG-36.17	36.17	35.40	1.73	35.40	1.205	0.0184	65.420
	ZDGN-ASP-29.99	29.99	35.40	3.27	47.70	1.447	0.0165	97.785
	ZDGN-ASP-32.54	32.54	32.20	2.23	53.90	1.355	0.0161	83.952
	ZDGN-ASP-35.50	35.50	34.10	2.86	41.50	1.252	0.0204	61.374
	ZDGN-ASPG-29.68	29.68	34.00	2.22	33.40	1.415	0.0127	111.408
	ZDGN-ASPG-32.66	32.66	34.10	2.75	35.40	1.370	0.0152	90.129
	ZDGN-ASPG-36.23	36.23	35.40	2.51	33.40	1.272	0.0194	65.559

In summary, the design results show that the new airfoil family obtained through the optimization of this paper has good aerodynamic performance under both design and non-design conditions, verifying the feasibility of the optimization design method.

C. OPTIMIZATIONS OF AIRFOIL SHAPES AT DIFFERENT REYNOLDS NUMBERS

The Reynolds number of the airfoil at different radius sections of the wind turbine blade is different, and the magnitude of the Reynolds number will change the flow state of the airfoil boundary layer, thus affecting the aerodynamic characteristics of the wind turbine blade airfoil, so it is necessary to optimize the airfoil shapes for different Reynolds numbers. Considering the actual operating conditions of commonly used wind turbines, two cases of Reynolds number Re=1e6 and Re=5e6 were taken to optimize the NACA634XX series airfoil. The optimization algorithm is PSOGA, and the optimization mathematical model only changes the Reynolds number. Due to space limitations, NACA63415, NACA63424 and NACA63430 are selected as the initial airfoils for optimization. Figs. 11 to 13 show the distribution of aerodynamic characteristics and pressure coefficients before and after optimization of the three airfoils at two Reynolds numbers, where T, Cp, Cl and Cl/Cd represent the differentials in geometric data, pressure coefficient, lift coefficient and lift-drag ratio between the optimized and initial airfoils at the same Reynolds number respectively. Table 3 shows the geometrical characteristics of the optimized airfoil family at different Reynolds numbers and the aerodynamic data at the set angle of attack. The new optimized airfoil is named ZDGN-ASYY-XXXX, where YY represents the Reynolds number, where R1 represents the Reynolds number of 1e6, R5 represents the Reynolds number of 5e6 and XXXX represents the maximum relative thickness of the airfoil.

Compared to the initial airfoil, most of the optimized airfoils have a reduced maximum relative thickness, an increased maximum relative curvature, a forward shift in the maximum thickness and maximum curvature positions, and an increased lift coefficient and lift-to-drag ratio at the set angle of attack. Under the condition that the Reynolds number is 1e6 in the whole range of attack angle from 0° to 20°, the maximum lift coefficients for the new airfoil are 1.493, 1.478 and 1.456, with differences in the maximum lift coefficients are 0.003, 0.126 and 0.103, and the maximum lift-to-drag ratios are 122.409, 119.935 and 84.243, respectively, with differences in maximum lift-to-drag ratios of 5.592, 13.512 5.530; under the condition that the Reynolds number is 5e6, the maximum lift coefficients for the three airfoils are 1.880, 1.646 and 1.495, with differences of 0.116, 0.131 and 0.102,, and the maximum lift-to-drag ratios are 172.723, 160.212 and 146.618, respectively, with differences of 19.431, 7.968 and 18.578. The trend in the graph shows that the maximum lift coefficient and the maximum lift-to-drag ratio of the optimized airfoil both increase with the increase in Reynolds number, the pressure coefficient distribution improves with the increase in Reynolds number and the pressure changes more smoothly, which helps to improve the force performance of the airfoil.

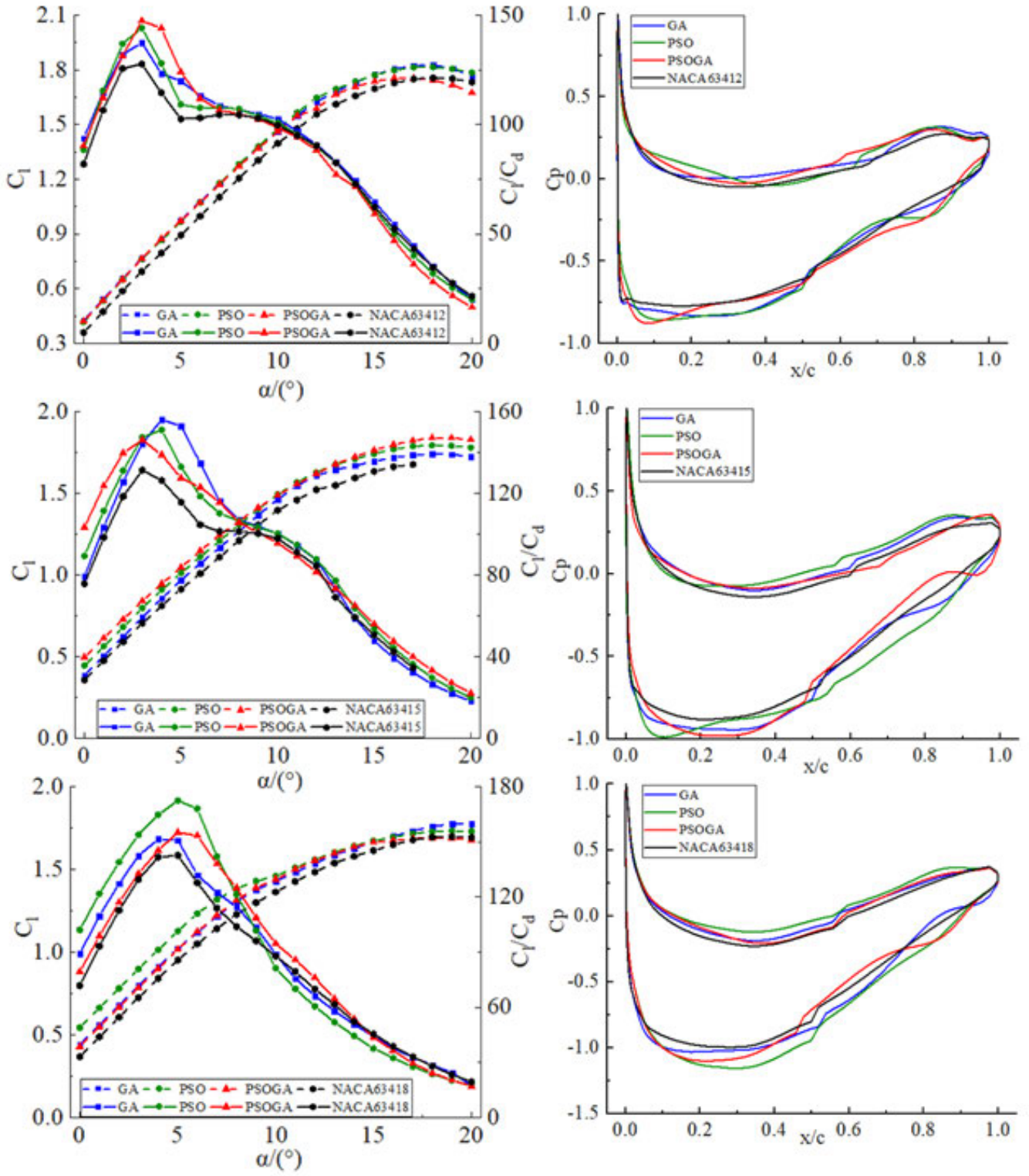

FIGURE 8. Comparison of aerodynamic characteristics of the blade tip airfoil with pressure coefficients at 2° angle of attack.

D. OPTIMIZATIONS OF AIRFOIL SHAPES AT DIFFERENT WEIGHTING FACTORS

In the optimization mathematical model of the airfoil family, the selection of the weight coefficient has an important impact on the optimization results. According to the design requirements of wind turbine blade airfoil, the weight coefficient q1=0.3, q2=0.7, and q1=0.8, q2=0.2 are selected to optimize the NACA634XX series airfoil, and the optimization

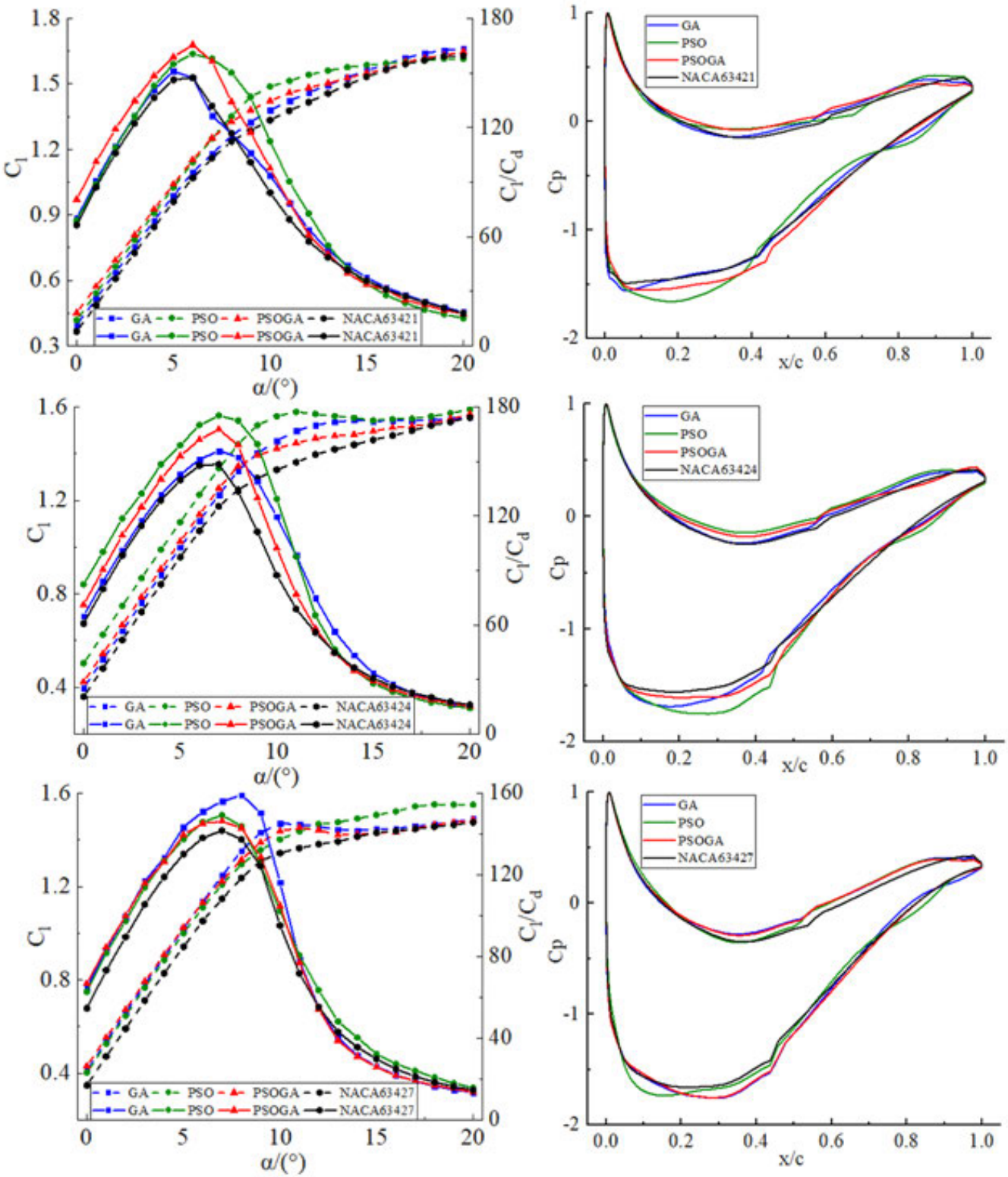

FIGURE 9. Comparison of aerodynamic characteristics of the mid-blade airfoil with pressure coefficients at 5° angle of attack.

algorithm adopts PSOGA. The optimized mathematical model only changes the weight coefficient in the objective function, and the rest remains unchanged. Figs. 14∼15 shows the comparison between aerodynamic characteristics and pressure coefficient of the optimized airfoil under different weight coefficients. Table 4 shows the geometric feature

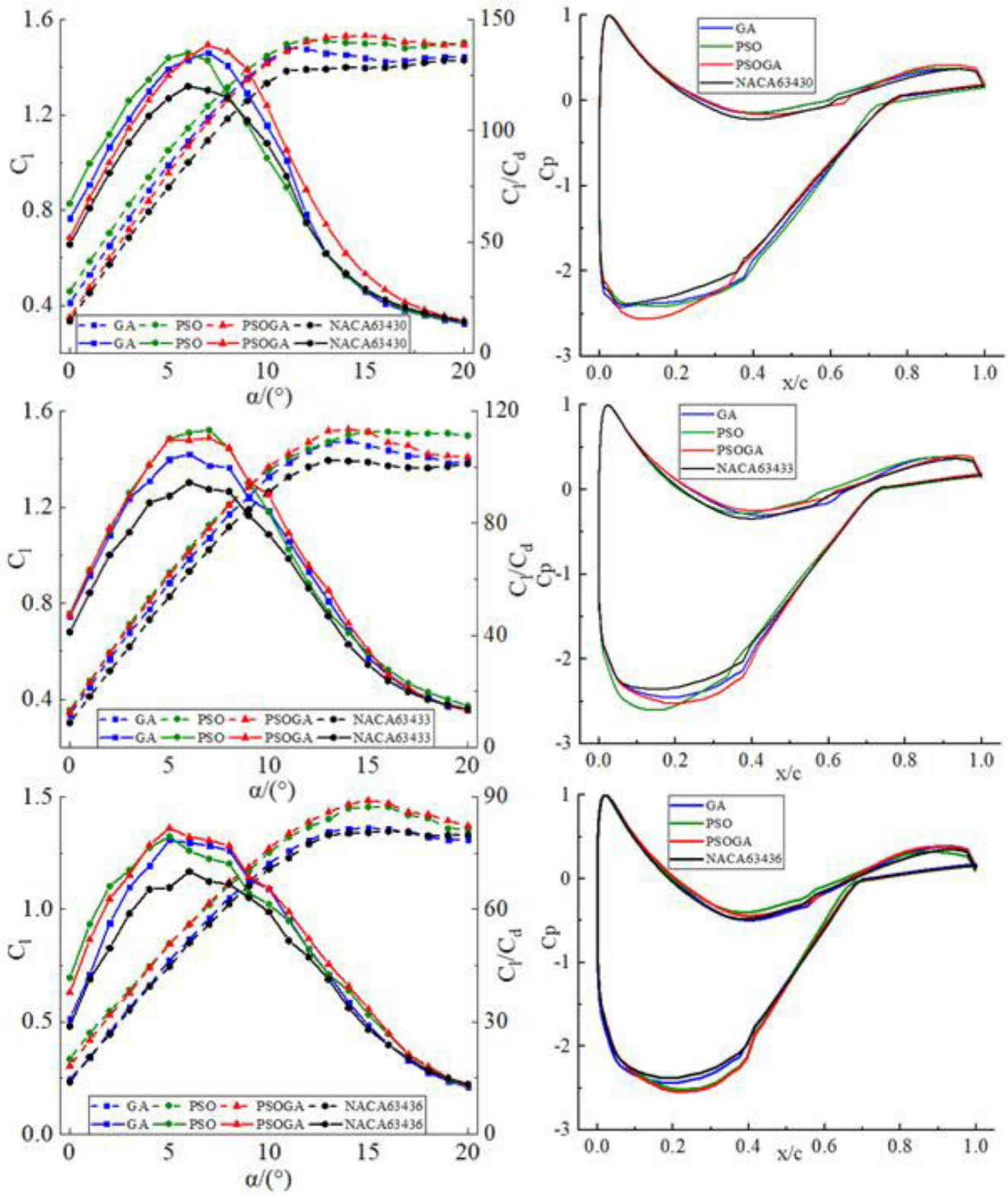

FIGURE 10. Comparison of aerodynamic characteristics of the blade root airfoil with pressure coefficients at 10° angle of attack.

parameters of the optimized airfoil family and aerodynamic data under the set Angle of attack. Under different weight coefficients, the optimized new airfoil is named ZDGN-ASYY-XXXX, where YY represents the weight coefficient,

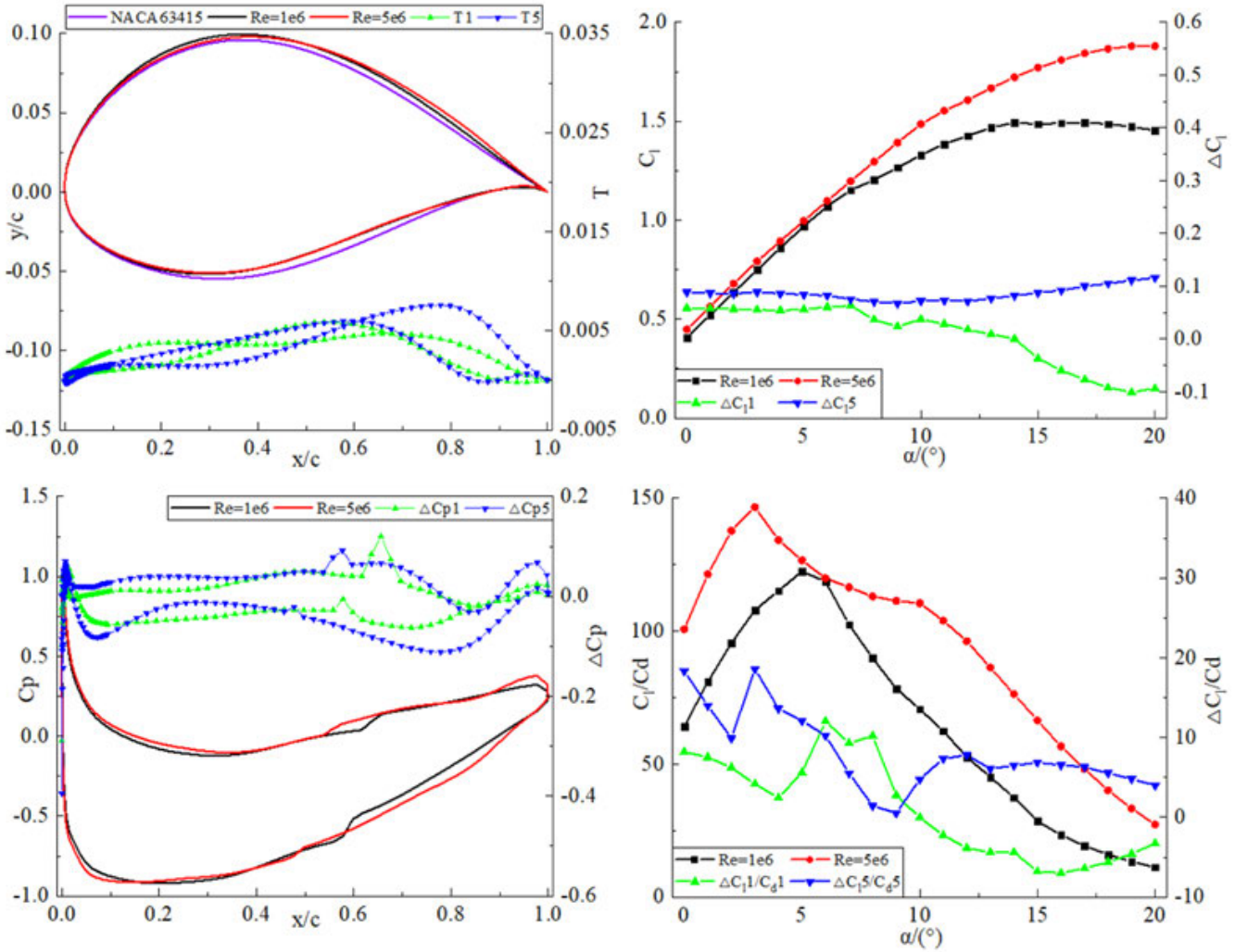

FIGURE 11. Comparison of aerodynamic characteristics before and after optimization of NACA63415 at different Reynolds numbers and pressure coefficients at 2° angle of attack.

where Q3 represents the weight coefficient q1=0.3, q2=0.7, Q8 represents the weight coefficient q1=0.8, q2=0.2, and XXXX represents the maximum relative thickness of the airfoil.

Compared to the initial airfoil, most of the new airfoils have a reduced maximum relative thickness, an increased maximum relative curvature, a forward shift in the position of the maximum thickness and maximum curvature. The lift coefficient is increased by 1.2% to 14.7% at the set angle of attack, and the lift-to-drag ratio is increased by 2.6% to 23%. In the whole range of attack angle from 0° to 20°, with weight coefficient q1=0.3 and q2=0.7, the maximum lift coefficients of the optimized airfoil family are 1.807, 1.730, 1.747, 1.694, 1.552, 1.563, 1.424, 1.401 and 1.508, respectively, the maximum lift-to-drag ratios are 148.267, 148.394, 154.791, 151.166, 155.203, 155.783, 133.145, 108.072 and 86.633, respectively. With the weight coefficient q1=0.8 and q2=0.2, the maximum lift coefficients of the optimized airfoil family are 1.792, 1.765, 1.697, 1.637, 1.563, 1.564, 1.440, 1.394 and 1.350, respectively, the maximum lift-to-drag ratios are 140.989, 151.037, 151.519, 154.098, 152.636, 156.783, 129.389, 107.953 and 87.447, respectively. Due to the different emphasis of the objective function on lift coefficient and lift-drag ratio in the optimization design, the obtained geometric parameters, aerodynamic parameters and pressure distribution of the optimized airfoil family are different, which need to be selected based on the design requirements in practical application.

VII. ACTUAL BLADE PERFORMANCE VERIFICATIONS

A. NEW AIRFOIL FAMILY BLADE RECONSTRUCTIONS MODELING

To verify the universality and replaceability of the new airfoil family on the actual blades, the wind turbine power of 1.2 MW, a blade length of 29 m, a maximum chord length of 2.43 m and a maximum twist angle of 13° was selected, with the blade airfoil type NACA634XX and the

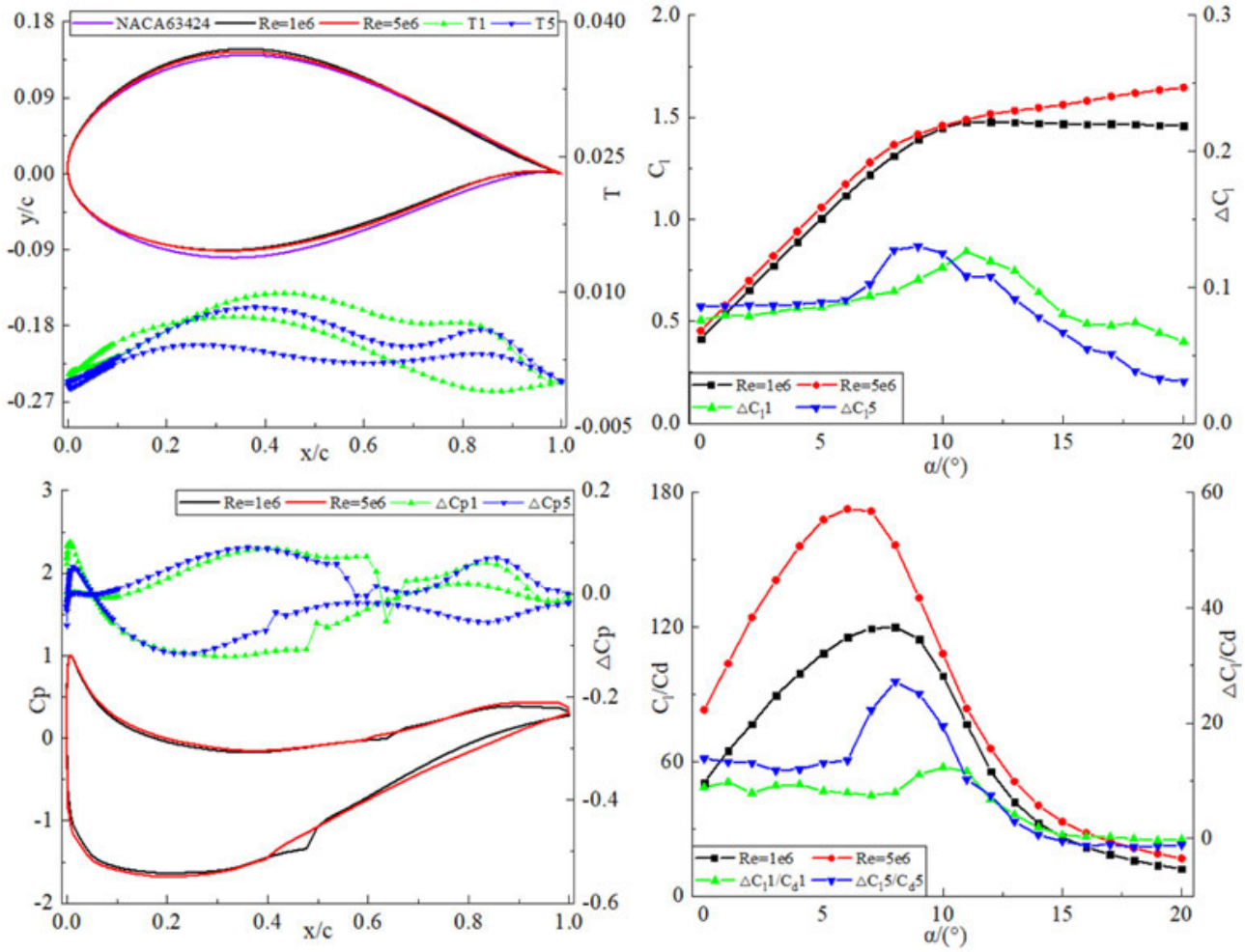

FIGURE 12. Comparison of aerodynamic characteristics before and after optimization of NACA63424 at different Reynolds numbers and pressure coefficients at 5° angle of attack.

TABLE 3. Geometric feature parameters and aerodynamic data of the optimized airfoil family with different reynolds numbers.

Airfoil Family		T_m/%	x_{tm}/%	*Cam*/%	x_{cam}/%	Cl	Cl/Cd	△Cl /%	△Cl/Cd /%
	ZDGN-ASR1-12.09	12.09	33.90	2.78	57.80	0.668	111.364	15.7	13.1
	ZDGN-ASR1-15.01	15.01	33.60	2.71	53.80	0.636	95.514	9.8	7.0
the Blade	ZDGN-ASR1-17.62	17.62	35.60	3.06	45.70	0.673	95.619	14.0	15.9
Tip Airfoil	ZDGN-ASR5-11.50	11.50	31.90	2.74	43.70	0.671	141.726	14.2	9.5
	ZDGN-ASR5-14.77	14.77	34.00	2.75	57.80	0.679	137.742	14.4	7.7
	ZDGN-ASR5-18.37	18.37	34.00	2.22	33.50	0.669	127.655	9.0	2.1
	ZDGN-ASR1-20.63	20.63	34.00	2.85	43.70	1.030	117.104	10.5	7.2
	ZDGN-ASR1-23.80	23.80	34.00	3.01	45.60	1.004	108.447	9.3	8.2
the Mid-	ZDGN-ASR1-26.88	26.88	34.00	2.54	55.80	0.986	98.459	2.7	23.1
Blade Airfoil	ZDGN-ASR5-20.59	20.59	34.00	3.07	45.70	1.075	181.73	11.2	21.1
	ZDGN-ASR5-23.56	23.56	34.00	2.73	43.60	1.058	167.966	9.2	8.5
	ZDGN-ASR5-26.59	26.59	35.50	2.40	39.50	1.054	161.865	2.5	28.4
	ZDGN-ASR1-29.50	29.50	34.10	2.20	35.40	1.299	73.549	4.2	8.0
	ZDGN-ASR1-32.62	32.62	34.10	2.53	47.70	1.247	62.005	7.1	13.5
the Blade	ZDGN-ASR1-35.54	35.54	34.20	2.56	31.30	1.128	43.209	5.8	1.6
Root Airfoil	ZDGN-ASR5-30.09	30.09	35.50	3.04	37.50	1.436	104.085	6.4	2.8
	ZDGN-ASR5-32.61	32.61	34.20	2.37	47.70	1.411	104.918	8.0	18.3
	ZDGN-ASR5-35.69	35.69	34.10	2.94	39.50	1.330	88.087	7.8	24.3

aerodynamic parameters shown in Fig. 16. Only the replacement of the relevant airfoil is considered, without considering the optimization of the chord length, twist angle and relative thickness.

B. COMPARATIVE ANALYSIS OF AERODYNAMIC PERFORMANCE

GH-Bladed software was applied to analyze the aerodynamic characteristics of the blade, mainly to study the output power

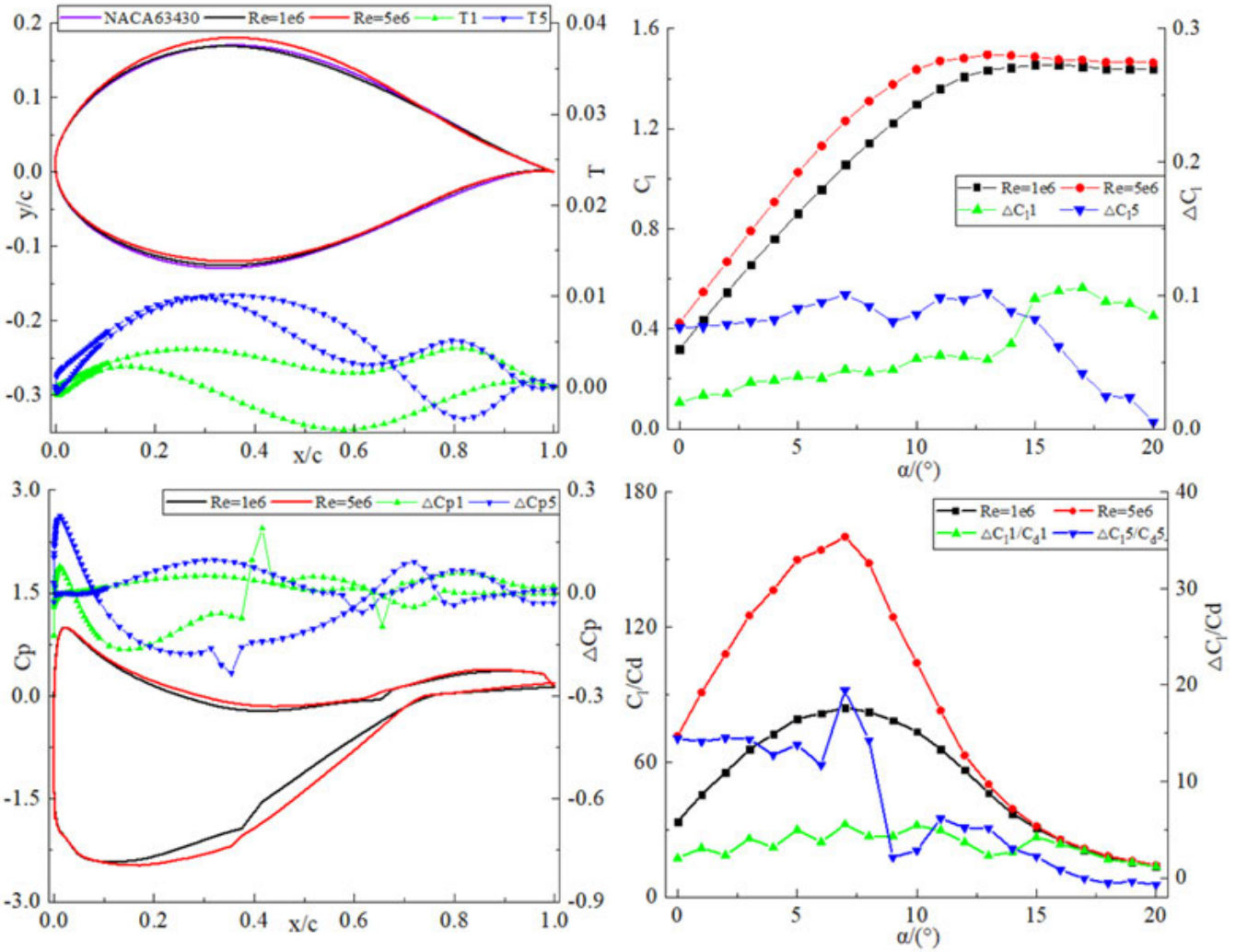

FIGURE 13. Comparison of aerodynamic characteristics before and after optimization of NACA63430 at different Reynolds numbers and pressure coefficients at 10° angle of attack.

TABLE 4. Geometric feature parameters and aerodynamic data of the optimized airfoil family with different weighting factors.

Airfoil Family		T_m/%	x_{tm}/%	*Cam*/%	x_{cam}/%	Cl	Cl/Cd	ΔCl /%	ΔCl/Cd /%
the Blade Tip Airfoil	ZDGN-ASQ3-11.86	11.86	33.70	2.58	47.70	0.637	134.557	8.7	7.0
	ZDGN-ASQ3-15.10	15.10	33.90	2.42	39.60	0.618	123.648	4.7	4.3
	ZDGN-ASQ3-17.76	17.76	33.50	2.54	45.70	0.666	120.151	9.7	6.6
	ZDGN-ASQ8-11.69	11.69	35.90	2.61	49.70	0.642	140.989	9.6	12.1
	ZDGN-ASQ8-15.27	15.27	33.60	2.67	47.70	0.677	126.075	14.7	6.4
	ZDGN-ASQ8-18.00	18.00	33.60	2.51	51.80	0.667	116.166	9.9	3.0
the Mid-Blade Airfoil	ZDGN-ASQ3-21.08	21.08	34.00	2.75	59.90	1.051	150.120	9.5	2.6
	ZDGN-ASQ3-23.89	23.89	35.50	2.92	47.70	1.023	145.391	6.9	4.0
	ZDGN-ASQ3-26.62	26.62	34.10	2.50	57.90	1.032	144.546	9.4	10.1
	ZDGN-ASQ8-20.76	20.76	33.60	2.33	45.70	0.971	150.226	1.2	2.7
	ZDGN-ASQ8-23.98	23.98	35.50	2.10	45.60	0.995	144.047	4.0	3.0
	ZDGN-ASQ8-26.62	26.32	34.20	2.49	47.90	0.962	140.546	2.0	8.0
the Blade Root Airfoil	ZDGN-ASQ3-30.03	30.03	35.40	2.38	47.70	1.374	97.975	3.0	3.7
	ZDGN-ASQ3-32.59	32.57	34.10	2.51	41.60	1.357	93.542	7.3	23.0
	ZDGN-ASQ3-35.69	35.69	34.10	2.94	39.50	1.316	65.393	11.5	10.2
	ZDGN-ASQ8-30.11	30.11	34.00	2.40	45.60	1.411	113.365	5.8	20.0
	ZDGN-ASQ8-32.53	32.53	34.10	2.76	45.60	1.353	86.198	7.0	13.3
	ZDGN-ASQ8-35.69	35.69	34.10	1.90	58.00	1.232	68.343	4.4	15.2

and wind energy utilization coefficient under different incoming wind velocity and blade tip speed ratio variable working conditions, to verify the feasibility of the optimized new airfoil family in the blade design, the calculation results are

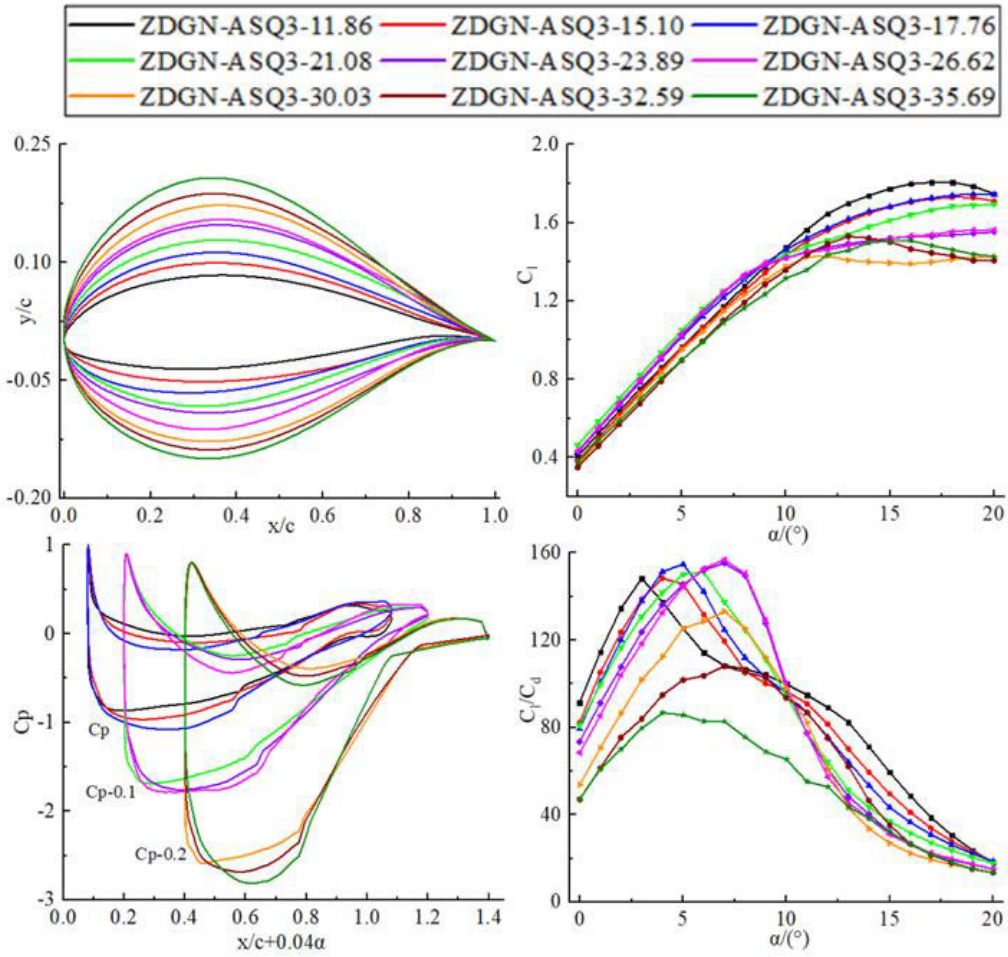

FIGURE 14. Comparison of optimized aerodynamic characteristics and pressure coefficients for weighting factors q1= 0.3, q2=0.7.

TABLE 5. Comparison of the new blade and initial blade output power and wind energy utilization coefficient.

Airfoil Family	Wind Speed (m/s)								Tip Speed Ratio					
	8		9		10		11		5		6		7	
	△	%	△	%	△	%	△	%	△	%	△	%	△	%
ZDGN-ASG-XXXX	0.023	7.6	0.033	7.4	0.046	7.3	0.061	7.2	0.022	6.2	0.018	4.1	0.001	0.2
ZDGN-ASP-XXXX	0.024	7.9	0.053	11.9	0.072	11.5	0.094	11.1	0.023	6.4	0.024	5.5	0.002	0.4
ZDGN-ASPG-XXXX	0.025	8.3	0.037	8.3	0.051	8.1	0.069	8.1	0.022	6.2	0.022	5.0	0.003	0.6
ZDGN-ASQ3-XXXX	0.018	5.9	0.025	5.6	0.034	5.4	0.045	5.3	0.019	5.3	0.011	2.5	0.003	0.6
ZDGN-ASQ8-XXXX	0.016	5.3	0.023	5.2	0.032	5.1	0.043	5.1	0.018	5.0	0.012	2.7	0.003	0.6
ZDGN-ASR1-XXXX	0.044	16.9	0.060	15.4	0.083	15.1	0.111	14.8	0.012	3.5	0.013	3.0	0.002	0.4
ZDGN-ASR5-XXXX	0.026	8.4	0.040	8.8	0.056	8.8	0.075	8.7	0.017	4.6	0.012	2.6	0.002	0.4

shown in Figs. 17 ∼ 18. The rated wind speed of the new blades (ZDGN-ASG-XXXX, ZDGN-ASP-XXXX, ZDGN-ASG-XXXX, ZDGN-ASQ3-XXXX, ZDGN-ASQ8-XXXX, ZDGN-ASR5-XXXX) is 12m/s. The rated wind speed of the new blade (ZDGN-ASR1-XXXX) is 11.5m/s. When the wind speed of the new blade is 11.5m/s, the output power of the new blade increases the most than that of the initial blade, which is 0.070MW, 0.107MW, 0.079MW, 0.052MW, 0.050MW, 0.127MW and 0.085MW, respectively. Compared with the initial blade, it increased by 7.172%, 10.963%, 8.094%, 5.328%, 5.123%, 14.767% and 8.621%.

Generally, the tip speed ratio of a three-blade wind turbine is about 5 ∼ 8. When the Reynolds number is 1e6, the optimal tip speed ratio of the initial blade is 7.3 and the maximum wind energy utilization coefficient is 0.471, and the optimal tip speed ratio of the new blade (ZDGN-ASR1-XXXX) is 7 and the maximum wind energy utilization coefficient is 0.472. When the Reynolds

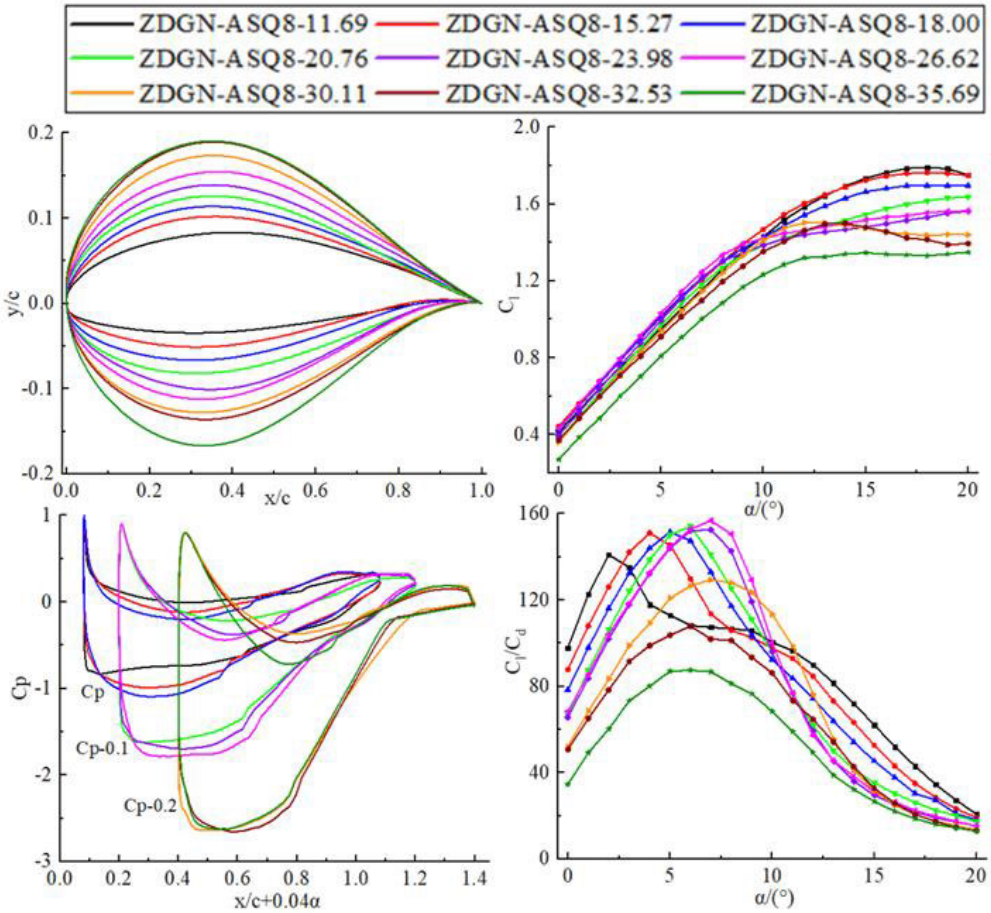

FIGURE 15. Comparison of optimized aerodynamic characteristics and pressure coefficients for weighting factors q1= 0.8, q2=0.2.

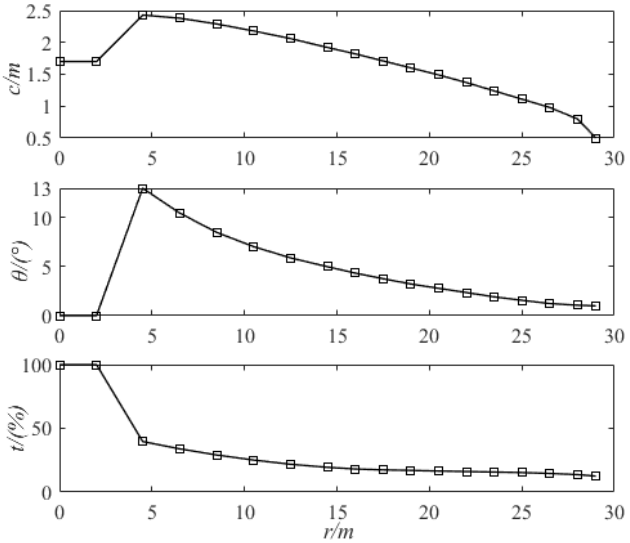

FIGURE 16. Aerodynamic profile parameters of blades.

number is 3e6, the optimal tip ratio of the initial blade is 7.2, and the maximum wind energy utilization coefficient is 0.477, the optimal tip ratios of the new blades (ZDGN-ASG-XXXX, ZDGN-ASP-XXXX, ZDGN-ASPG-XXXX, ZDGN-ASQ3-XXXX, ZDGN-ASQ8-XXXX) are 7, 6.8, 7, 7 and 7, respectively, and the maximum wind energy utilization coefficients were 0.478, 0.478, 0.480, 0.480, 0.480. When the Reynolds number is 5e6, the optimal tip speed ratio of the initial blade is 7.2, the maximum wind energy utilization coefficient is 0.479, and the optimal tip speed ratio of the new blade (ZDGN-ASR5-XXXX) is 7, and the maximum wind energy utilization coefficient is 0.480.

In this paper, the power obtained by the new airfoil family in the wind speed range of 3 $\sim$ 7m/s is not much different from that of the initial blade. The power obtained in the wind speed range of 8$\sim$11m/s and the wind energy utilization coefficient obtained at the tip speed ratios range of 5 $\sim$ 7 are compared with those of the initial blade, as shown in Table 5, where $\triangle$ and % represent the difference values and percentages of improvement compared with those of the initial blade. It can be seen that under the same working conditions, the output power and wind energy utilization coefficient of the new blade is significantly improved. In addition, the aerodynamic shape of the new blade is not the best aerodynamic shape corresponding to the new airfoil family. If the new airfoil family is optimized, the blade performance will be more improved.

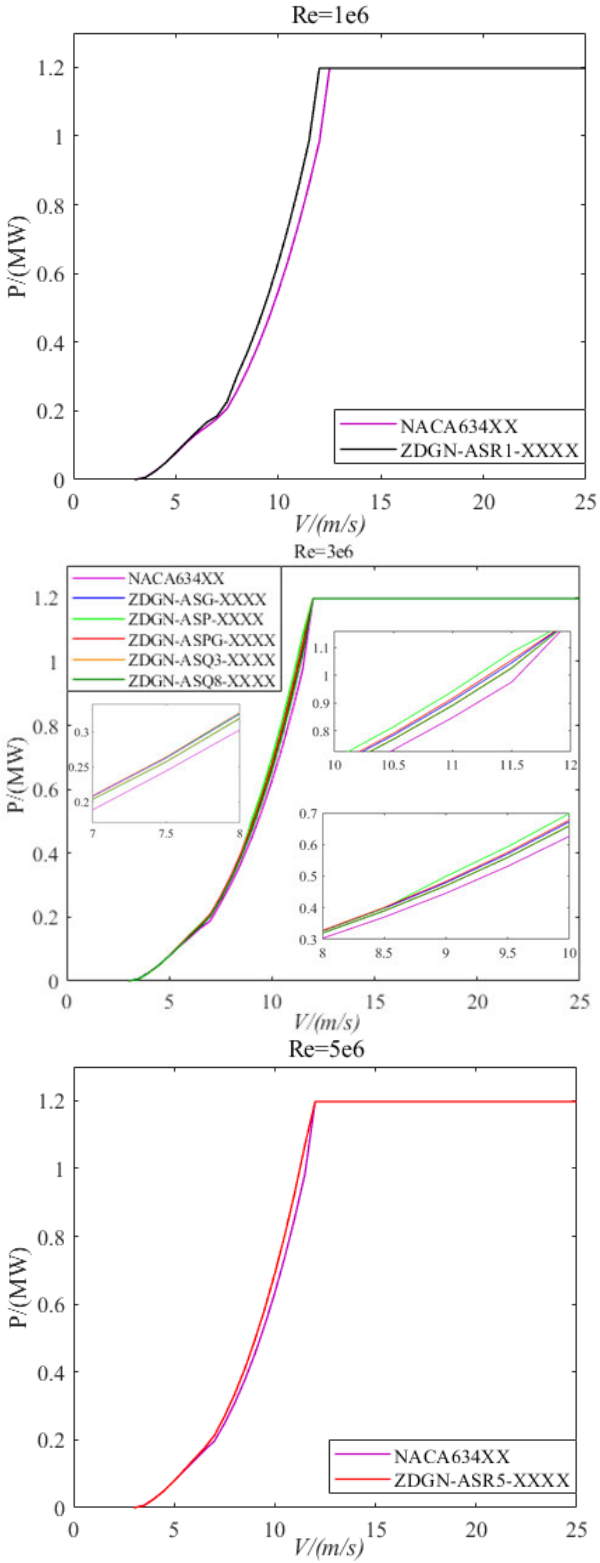

FIGURE 17. Comparison of wind power curves.

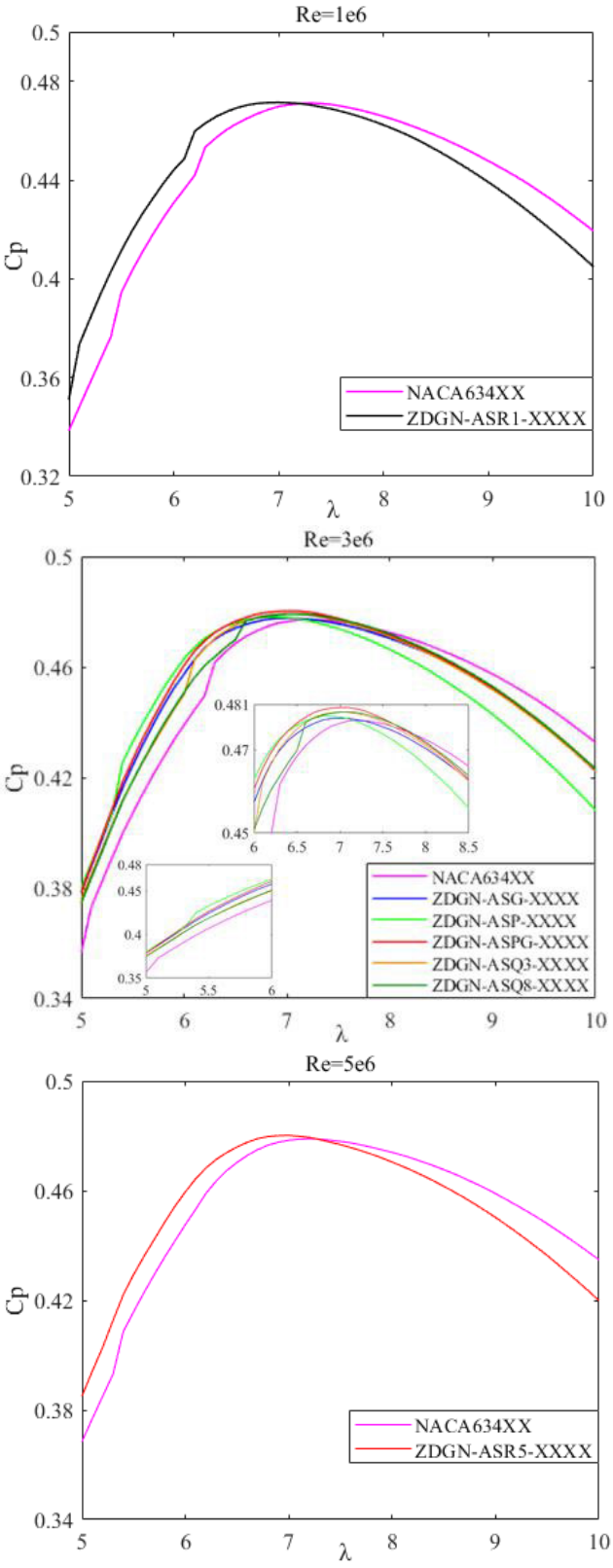

FIGURE 18. Comparison of wind energy utilization coefficient.

VIII. CONCLUSION

1) A single-objective optimization mathematical model of a high-performance wind turbine blade airfoil family is established, and seven groups of airfoil families (ZDGN-ASG, ZDGN-ASP, ZDGN-ASPG, ZDGN-ASR1, ZDGN-ASR5, ZDGN-ASQ3 and ZDGN-ASQ8) are obtained by considering different angles of

TABLE 6. Summary of work on wind turbine blade airfoil optimization.

Airfoil	Tool	Parameterization method	Optimization Algorithm	Objective Function	Design Variable	Constraint Condition	Findings	Ref.
S809	CFD	Hicks-Henne	GA+Kriging	Maximum average lift-to-drag ratio and Minimum range of lift-to-drag ratio fluctuations.	c_k	$c_k \in [-0.006,0.006]$ $UR \in [-0.0015, 0.0015]$ $TI \in [0.0375,0.2625]$	The standard deviation fluctuation range of the optimal airfoil lift-to-drag ratio is reduced by 17.96%, with no decrease in the average lift-to-drag ratio.	Tang, et al. [11]
NACA-9415	XFOIL	PARSEC	GA	Max(Cl)	12 geometric parameters	$y_{te}=0$ $\triangle y_{te}=0$ $Cl>1$	At an angle of attack of 0°, the lift coefficients for the NACA-9415 and optimized airfoils are 0.93 and 1.1 respectively, with lift-to-drag ratios of 106 and 142 respectively.	Saleem, et al. [12]
USP07-45XX	HARP_Opt	Bezier curve	GA	$F(B(u),\mathrm{Re}) = \sum_{i=1}^{n}(\frac{Cl_i}{Cd_i*1.1})\times\frac{1}{m}$	p_i	$Y(u)_{upper}$-$Y(u)_{lower}>0$ $0.14>(Y(u)_{upper}$ $Y(u)_{lower})>0.08$ $(Y(u)_{upper}) \leq 0.2$ $Y(u)_{lower} \geq -0.1$	The optimized airfoil USP07-4510 has very little variation in lift coefficient in both smooth and rough conditions and the lift-to-drag ratio is better than SG6043 in both cases.	Ram, et al. [13]
DU97-W-300	RFOIL	B spline curve	GA+Isight	$f_{obj}=w_i p_i f_a$	T C_{am} X_t X_{cam} T_{tr}	$T=0.35$ $cl_{design}>1.1$ $\alpha_{stall}<15$ $c_{l,max}<1.85$ $M_{stallx}<350$ $c_{l,max,ft}>0.8$ $S_{re,ld}<0.8$	The new airfoil has a high design lift coefficient, an acceptable maximum lift-to-drag ratio, moderate stall parameters and ideal stability parameters.	Li, et al. [14]
GA(W)-1	CFD	Bezier curve	GA+ANN	Max(Cl / Cd)	p_i	The maximum thickness is about 0.17c and the minimum thickness is 0.025c at 0.9c	The optimized airfoil has a lift-to-drag ratio of approximately 100 and the artificial neural network is able to model airfoils with the high angle of attack, reducing the computational time by almost 50%.	Ribeiro, et al. [15]
WQ-A	RFOIL	Airfoil functional integral theory	PSO	The lift-to-drag ratio of smooth and rough operating conditions is maximized under multiple attack angles.	$\varphi(\theta)$	$X_{min} \leq X \leq X_{max}$ $t_{15} \in [0.148,0.152]$ $t_{18} \in [0.178,0.182]$ $t_{21} \in [0.208,0.212]$ $0.24 \leq L_{max} \leq 0.35$ airfoil pressure side: $-5 \leq C \leq 1$ $-2 \leq C' \leq 10$ airfoil suction side: $-1 \leq C \leq 5$ $-10 \leq C' \leq 2$ $t\|_{x=0.1} \geq 0.08$	The WQ-B210 airfoil exhibits a better average lift-to-drag ratio in the range of 2° to 12° angle of attack, an improvement of approximately 6.25%.	Wang, et al. [16]

TABLE 6. *(Continued.)* **Summary of work on wind turbine blade airfoil optimization.**

Airfoil	Tool	Parameterization method	Optimization Algoruthm	Objective Function	Design Variable	Constraint Condition	Findings	Ref.
S818 S825 S826	XFOIL	CST	PSO	Maximum power generation from blades.	shape function coefficient	Thickness of optimized airfoil ⩽ thickness of original airfoil	According to IBEM results, the optimized airfoil shape increases the wind turbine's power production by 2.68%.	Kavian i, et al. [17]
Risø-A1-15	XFOIL	Airfoil functional integral theory+Hicks-Henne	PSO	The maximum value of the linearly weighted sum of lift-to-drag ratios at different angles of attack is taken as the objective.	Top 10 items Coefficients	$0.2 < x_t < 0.3$	The new airfoil has an average lift coefficient increase of 38.62% and 6.48% and a maximum lift-to-drag ratio increase of 6.02% and 1.75% respectively.	Ju, et al. [18]
NACA 64618	RFOIL	Airfoil functional integral theory	PSO	$\min F_{obj}=F_p+F\varepsilon+F_c$	a_k b_k k=3	$0.179 < th < 0.181$	The new airfoil shape helps to reduce the torsional displacement of the blade tip and improves the ability to inhibit the torsional of the blade.	Chen, et al. [19]
NACA 4418	XFOIL	3-order spline curve	GA+SA	Max(*Cl / Cd)*	x,y, β1 β2 14 variables in total	Airfoil thickness variation within 5%, maximum thickness at 0.24 to 0.35 of chord length.	The modified simulated annealing genetic algorithm optimizes the airfoil to achieve a 21.97% improvement in the lift-to-drag ratio and has a more uniform pressure distribution.	Liu, et al. [20]
S809	XFOIL	Bezier curve	GABP+ANN	Max(Cl) and Max(Cl / Cd) both exceed the original value.	8 control points	—	The drag coefficient of the optimized airfoil is unstable, the lift coefficient is better and the maximum lift-to-drag ratio is significantly better than the original airfoil.	Hao, et al. [21]
E387	XFOIL	Bezier curve	NSGA II	Improved lift-to-drag ratio at all operating conditions	8 control points	Range of variation of constraint control points	The optimized airfoil has less variance in lift-to-drag ratio and maintains similar characteristics to the original airfoil.	Wei, et al. [22]
S809	XFOIL	PARSEC	NE+GA	*Cl* 、 *Cd*	11 geometric parameters	PARSEC parameter range with 10% starting parameter variation without any geometric or aerodynamic constraints	After optimization, the airfoil thickness and curvature increase, and the lift coefficient increases.	Pierlui gi, et al. [23]
NREL VI and NREL 5 MW blade cross-section shape	CFD-CSD	Hicks-Henne	ANN+GA	Min(*COE)*	*ck*	Constrained maximum torque and thrust coefficient	Optimized energy cost reduction of 0.82% for NREL VI rotor blades and 1% for NREL 5 MW wind turbine blades.	Lee, et al. [24]

TABLE 6. *(Continued.)* **Summary of work on wind turbine blade airfoil optimization.**

Airfoil	Tool	Parameterization method	Optimization Algoruthm	Objective Function	Design Variable	Constraint Condition	Findings	Ref.
NACA 4412	KJ	Fourth-order polynomial function	CSA	Fmax=107N is the target lift	P_i	Imax=2×10^3 is the upper limit of optimization iteration	The average lift-to-drag ratio coefficient and maximum lift-to-drag ratio coefficient of the CSA-KJ4412 airfoil have increased, with a 4.53% increase in the average lift-to-drag ratio over the NACA4412.	Zhang, et al. [25]
S809	MATLAB+XFOIL	CST+PARSEC	GA	Max(*Cl*) Max(*Cl / Cd*)	Control coefficients	Geometric constraints, aerodynamic constraints, optimization criteria	The airfoil lift coefficient increased by 11.8% and lift-to-drag ratio increased by 9.6% with CST optimization, while the airfoil lift coefficient increased by 10% and lift-to-drag ratio decreased by 2% with PARSEC optimization.	Akram, et al. [26]
DU21-A17	XFOIL	Bezier curve	RSM+ANN +GA	Max(*Cl / Cd*)	8 control points	Constrains the range of variation of the control point, constrains the minimum thickness value	The prediction accuracy of the agent model computed by ANN is higher when the provided dataset has high complexity, but the accuracy of RSM decreases when the dataset complexity is lower.	Sahuck Oh, et al. [27]
S822	CFD	Hermite curve	RSM+BiMADS	Max(T) Min(σ)	P_i、I_{ij}	—	High thrust and improved aerodynamic stability can be achieved by modifying the blade shape.	Benim, et al. [28]
CU-W1-XX	XFOIL	Bezier curve	GA	Max(*Cl / Cd*)	13 control points	Minimum trailing edge thickness 0.5% Maximum thickness location geometrically constrained between x/c = 0.27 to 0.32, Max(Cl) ≥ 1.9	The new airfoil CU-W1-XX series offer the same or better performance.	Miller, et al. [29]
NACA 4415	GRNN	NACA four-position airfoil calculation equation + CST	PSO	Max(*Cl / Cd*)	13-dimensional CST parameterized coefficients	Maximum relative thickness 15%, maximum relative curvature 1% to 6%, maximum relative curvature position 20% to 50%.	The new airfoil offers a 6.96% increase in maximum lift coefficient and a 7.37% increase in maximum lift-to-drag ratio over the main operating angle of attack range.	Ju, et al. [30]

attack, different Reynolds numbers and different weighting coefficients. Their lift coefficients and lift-to-drag ratios are better than those of the initial airfoil family in both design and non-design conditions.

2) The maximum relative thickness of the optimized new airfoil is decreased, the maximum relative curvature is increased, and the maximum thickness position and maximum curvature position are shifted forward. The maximum lift coefficient and maximum lift-to-drag ratio are higher than those of the initial airfoil at different angles of attack, different Reynolds numbers and different weighting factors, and they increase with the Reynolds number.
3) When the new airfoil family is applied to the actual 1.2MW blade, the output power and wind energy utilization coefficient of the new blade are significantly improved. It is proved that the new airfoil family has a wide range of universality and replaceability and has a good engineering application prospect.

IX. FURTHER WORK

In order to design a wind turbine blade that meets the requirements of high efficiency and full performance, it is necessary to further consider embedding the structural attributes into the airfoil family optimization mathematical model, so as to obtain a new airfoil family with both aerodynamic and structural advantages. At the same time, it is necessary to carry out the wind tunnel experiments and field experiments to verify the aerodynamic performance of the new airfoil family and the wind energy capture ability of the new blade, in order to further demonstrate the accuracy of the optimization model and the practicability of the new airfoil family.

APPENDIX

See Table 6.

REFERENCES

[1] Z. Zhang, W. Li, and X. Jia, "CFD investigation of a mobula birostris-based bionic vortex generator on mitigating the influence of surface roughness sensitivity of a wind turbine airfoil," *IEEE Access*, vol. 8, pp. 223889–223896, 2020.
[2] A. Chehouri, R. Younes, A. Ilinca, and J. Perron, "Review of performance optimization techniques applied to wind turbines," *Appl. Energy*, vol. 142, pp. 361–388, Mar. 2015.
[3] Z. Han, Z. Gao, W. Song, and L. Xia, "On airfoil research and development: History, current status, and future directions," *Acta Aerodynamica Sinica*, vol. 39, no. 6, pp. 1–36, Jun. 2021.
[4] E. N. Jacobs, "Preliminary report on laminar-flow airfoils and new methods adopted for airfoil and boundary-layer investigations," U.S. Dept. Commerce, Nat. Tech. Inf. Service, Nat. Advisory Committee Aeronaut., Washington, DC, USA, Tech. Rep. NACA-WR-L-345, Jun. 1939.
[5] J. L. Tangle and D. M. Somers, "NREL airfoil families for HAWTs," in *Proc. WINDPOWER*, Washington, DC, USA, Jan. 1995, pp. 117–123.
[6] A. Björck, *Coordinates and Calculations for the FFA-W1-XXX, FFA-W2-xxx and FFA-W3-xxx Series of Airfoils for Horizontal Axis Wind Turbines*. Stockholm, Sweden: FFA, 1990.
[7] R. P. J. O. M. van Rooij and W. A. Timmer, "Roughness sensitivity considerations for thick rotor blade airfoils," *J. Sol. Energy Eng.*, vol. 125, no. 4, pp. 468–478, Nov. 2003.
[8] P. Fuglsong and C. Bak, "Development of the Risø wind turbine airfoils," *Wind Energy*, vol. 7, no. 2, pp. 145–162, Apr./Jun. 2004.
[9] Z. D. Qiao, W. P. Song, and Y. W. Gao, "Design and experiment of the NPU-WA airfoil family for wind turbines," *Acta Aerodynamica Sinica*, vol. 30, no. 2, pp. 260–265, 2012.
[10] T. Wang, L. Tian, W. Zhong, L. Wang, and C. Y. Zhu, "Aerodynamic research progress in wind energy I: Wind turbine aerodynamic characteristics," *Acta Aerodynamica Sinica*, vol. 40, no. 4, pp. 1–21, Aug. 2022.
[11] X. Tang, K. Yuan, N. Gu, P. Li, and R. Peng, "An interval quantification-based optimization approach for wind turbine airfoil under uncertainties," *Energy*, vol. 244, Apr. 2022, Art. no. 122623.
[12] A. Saleem and M.-H. Kim, "Aerodynamic performance optimization of an airfoil-based airborne wind turbine using genetic algorithm," *Energy*, vol. 203, Jul. 2020, Art. no. 117841.
[13] K. R. Ram, S. P. Lal, and M. R. Ahmed, "Design and optimization of airfoils and a 20 kW wind turbine using multi-objective genetic algorithm and HARP_Opt code," *Renew. Energy*, vol. 144, pp. 56–67, Dec. 2019.
[14] X. Li, K. Yang, J. Bai, and J. Xu, "A new optimization approach to improve the overall performance of thick wind turbine airfoils," *Energy*, vol. 116, pp. 202–213, Dec. 2016.
[15] A. F. P. Ribeiro, A. M. Awruch, and H. M. Gomes, "An airfoil optimization technique for wind turbines," *Appl. Math. Model.*, vol. 36, no. 10, pp. 4898–4907, Oct. 2012.
[16] Q. Wang, J. Wang, J. Sun, J. Ren, and Q. Wei, "Optimal design of wind turbine airfoils based on functional integral and curvature smooth continuous theory," *Aerosp. Sci. Technol.*, vol. 55, pp. 34–42, Aug. 2016.
[17] H. Kaviani and M. Moshfeghi, "Multi-megawatt horizontal axis wind turbine blade optimization based on PSO method," *Aerospace*, vol. 10, no. 2, p. 158, Feb. 2023.
[18] H. Ju, X. D. Wang, and J. H. Lu, "Aerodynamic optimization design of wind turbine airfoil based on hybrid parameterization and particle swarm algorithm," *Acta Energiae Solaris Sinica*, vol. 44, no. 5, pp. 473–479, 2023.
[19] G. Chen, J. Chen, Z. Y. Sun, and X. P. Pang, "Airfoil design for wind turbines based on static-aeroelastic performance," *Acta Energiae Solaris Sinica*, vol. 41, no. 6, pp. 8–15, 2020.
[20] H. Liu, Y. Wu, P. Zhang, and S. Hou, "Research on adaptive simulated annealing genetic algorithm in wind turbine airfoil optimization design," *Renew. Energy Resour.*, vol. 36, no. 6, pp. 930–934, 2018.
[21] H. Wen, S. Sang, C. Qiu, X. Du, X. Zhu, and Q. Shi, "A new optimization method of wind turbine airfoil performance based on Bessel equation and GABP artificial neural network," *Energy*, vol. 187, Nov. 2019, Art. no. 116106.
[22] X. Wei, X. Wang, and S. Chen, "Research on parameterization and optimization procedure of low-Reynolds-number airfoils based on genetic algorithm and Bezier curve," *Adv. Eng. Softw.*, vol. 149, Nov. 2020, Art. no. 102864.
[23] P. D. Vecchia, E. Daniele, and E. D'Amato, "An airfoil shape optimization technique coupling PARSEC parameterization and evolutionary algorithm," *Aerosp. Sci. Technol.*, vol. 32, no. 1, pp. 103–110, Jan. 2014.
[24] H. M. Lee and O. J. Kwon, "Performance improvement of horizontal axis wind turbines by aerodynamic shape optimization including aeroealstic deformation," *Renew. Energy*, vol. 147, pp. 2128–2140, Mar. 2020.
[25] J. Zhang, W. Guo, P. Zhang, and H. Ji, "Optimizing airfoil aerodynamic characteristics by using proposed CSA-KJ method," *Appl. Sci.*, vol. 13, no. 2, p. 924, Jan. 2023.
[26] M. T. Akram and M.-H. Kim, "Aerodynamic shape optimization of NREL S809 airfoil for wind turbine blades using Reynolds-averaged Navier Stokes model—Part II," *Appl. Sci.*, vol. 11, no. 5, p. 2211, Mar. 2021.
[27] S. Oh, "Comparison of a response surface method and artificial neural network in predicting the aerodynamic performance of a wind turbine airfoil and its optimization," *Appl. Sci.*, vol. 10, no. 18, p. 6277, Sep. 2020.
[28] A. Benim, M. Diederich, and B. Pfeiffelmann, "Aerodynamic optimization of airfoil profiles for small horizontal axis wind turbines," *Computation*, vol. 6, no. 2, p. 34, Apr. 2018.
[29] M. Miller, K. L. Slew, and E. Matida, "The development of a flatback wind turbine airfoil family," *Wind Energy*, vol. 21, no. 12, pp. 1372–1382, Dec. 2018.
[30] H. Ju, X. D. Wang, J. H. Lu, and X. S. Qin, "Rapid optimization design of wind turbine airfoil based on small sample neural network and multiple constraints," *J. Eng. Thermal Energy Power*, vol. 37, no. 11, pp. 176–184, 2022.
[31] Q. Sun, "Research on optimal design of airfoil for horizontal-axis wind turbines," M.S. thesis, Xiangtan Univ., Xiangtan, China, 2013.
[32] Y. Zhang, J. Q. Bai, and J. Zhu, "Application of improved Hicks–Henne shape function to airfoil parameterization," *Flight Dyn.*, vol. 29, no. 5, pp. 35–38, 2011.
[33] L. Yu, Z. K. Hu, and H. Cheng, "Multidisciplinary design optimization for wind turbine airfoil," *J. Nanjing Univ. Aeronaut. Astronaut.*, vol. 43, no. 5, pp. 697–700, 2011.
[34] B. Cheng and Y. Yao, "Design and optimization of a novel U-type vertical axis wind turbine with response surface and machine learning methodology," *Energy Convers. Manage.*, vol. 273, Dec. 2022, Art. no. 116409.
[35] Y. G. Liu, "Study on structural damage identification based on wavelet-particle swarm genetic optimization algorithm," M.S. thesis, Changsha Univ. Sci. Technol., Changsha, China, 2018.

ZHAOHUANG ZHANG received the M.D. degree in mechanical engineering from the Beijing Graduate School, North China Institute of Water Conservancy, in 1990, and the Ph.D. degree in management science and engineering from North China Electric Power University, Beijing, China, in 2008.

Currently, he is a Professor with North China Electric Power University. He has published nearly 100 academic articles, including more than 30 SCI and EI articles, published two academic works, and has obtained more than 20 national authorized invention patents. His current research interests include failure prevention in the working process of power machinery, operation theory and application of underground advanced construction equipment, and energy conversion safety and energy saving. He is a member of the Institution of Engineering and Technology and the National 863 Expert Database, the Jiangsu Science and Technology Consulting Expert, and the Beijing Science and Technology Award Review Expert.

DI GAO was born in Hebei, China, in 1993. She received the M.D. degree in mechanical engineering from North China Electric Power University, Beijing, China, in 2019, where she is currently pursuing the Ph.D. degree in power machinery and engineering.

Since 2019, she has been conducting research on the theory and application of the interaction between flowing air and wind turbine blades.

YUNFEI QI was born in Anhui, China, in 2000. He received the B.D. degree in mechanical design, manufacturing, and automation from Hefei University, Hefei, China, in 2022. He is currently pursuing the M.D. degree in mechanical engineering with North China Electric Power University, Beijing, China.

KEFENG CHENG was born in Shanxi, China, in 1998. He received the M.D. degree in mechanical engineering from North China Electric Power University, Beijing, China, in 2023, where he is currently pursuing the Ph.D. degree in mechanical engineering.

Since 2020, he has been conducting research on the operation theory and application of underground advanced construction equipment.